AFRL-RW-EG-TR-2012-114

A COMPARISON OF THE PERFORMANCE OF 2D SQUARE AND RECTANGULAR DIELECTRIC VEIN STRUCTURES

Douglas V. Nance

AFRL/RWWC
101 W. Eglin Blvd.
STE 334
Eglin AFB, FL 32542-6810

September 2012

INTERIM REPORT

AIR FORCE RESEARCH LABORATORY
MUNITIONS DIRECTORATE

■ **Air Force Materiel Command** ■ **United States Air Force** ■ **Eglin Air Force Base, FL 32542**

NOTICE AND SIGNATURE PAGE

Using Government drawings, specifications, or other data included in this document for any purpose other than Government procurement does not in any obligate the U.S. Government. The fact that the Government formulated or supplied the drawings, specifications, or other data does not license the holder or any other person or corporation, or convey any rights or permission to manufacture, use, or sell any patented invention that may relate to them.

This report was cleared for public release by the 96th Air Base Wing, Public Affairs Office, and is available to the general public, including foreign nationals. Copies may be obtained from the Defense Technical Information Center (DTIC) < http://www.dtic.mil/dtic/index/html>.

AFRL-RW-EG-TR-2012-114 HAS BEEN REVIEWED AND IS APPROVED FOR PUBLICATION IN ACCORDANCE WITH ASSIGNED DISTRIBUTION STATEMENT.

FOR THE DIRECTOR:

SIGNED	SIGNED
Craig R. Ewing, DR-IV, PhD	Douglas V. Nance
Technical Advisor	Research Scientist
Weapon Engagement Division	AFRL/RWWC

This report is published in the interest of scientific and technical information exchange, and its publication does not constitute the Government's approval or disapproval of its ideas or findings.

REPORT DOCUMENTATION PAGE

Form Approved
OMB No. 0704-0188

PLEASE DO NOT RETURN YOUR FORM TO THE ABOVE ADDRESS.

1. REPORT DATE *(DD-MM-YYYY)*	2. REPORT TYPE	3. DATES COVERED *(From - To)*
27-09-2012	INTERIM	01-01-2012 - 04-05-2012

4. TITLE AND SUBTITLE

A COMPARISON OF THE PERFORMANCE OF 2D SQUARE AND RECTANGULAR DIELECTRIC VEIN STRUCTURES

5a. CONTRACT NUMBER

5b. GRANT NUMBER

5c. PROGRAM ELEMENT NUMBER

62602F

6. AUTHOR(S)

Douglas V. Nance

5d. PROJECT NUMBER

2502

5e. TASK NUMBER

67

5f. WORK UNIT NUMBER

63

7. PERFORMING ORGANIZATION NAME(S) AND ADDRESS(ES)

AFRL/RWWC
101 W. Eglin Blvd., STE 334
Eglin AFB, FL 32542-6810

8. PERFORMING ORGANIZATION REPORT NUMBER

AFRL-RW-EG-TR-2012-114

9. SPONSORING/MONITORING AGENCY NAME(S) AND ADDRESS(ES)

AFRL/RWWC
101 W. Eglin Blvd., STE 334
Eglin AFB, FL 32542-6810

10. SPONSOR/MONITOR'S ACRONYM(S)

AFRL-RW-EG-TR

11. SPONSOR/MONITOR'S REPORT NUMBER(S)

AFRL-RW-EG-TR-2012-114

12. DISTRIBUTION/AVAILABILITY STATEMENT

DISTRIBUTION A. Approved for public release, distribution unlimited. (96ABW-2012-0395)

13. SUPPLEMENTARY NOTES

14. ABSTRACT

This technical report describes a computational research task performed to support continuing investigations into the electromagnetic behavior of photonic crystals. Simple dielectric vein structures are used to mimic the configuration of the photonic crystals found within the wings of the Green Hairstreak Butterfly, an insect noted for its use of photonic crystals for coloration. An earlier investigation employed a square dielectric vein structure to approximate these photonic crystals. In this case, the numerical model is improved. A rectangular vein structure is employed with two distinct values for the vein dielectric permittivity. The performance of the rectangular model is compared with that of the square model for both the Transverse Electric and Transverse Magnetic waves under mirror symmetry. The structure of attendant photonic bands is discussed.

15. SUBJECT TERMS

photonic crystal, Maxwell equations, dielectric, Bloch form

16. SECURITY CLASSIFICATION OF:			17. LIMITATION OF ABSTRACT	18. NUMBER OF PAGES	19a. NAME OF RESPONSIBLE PERSON
a. REPORT	b. ABSTRACT	c. THIS PAGE			Douglas V. Nance
UNCLAS	UNCLAS	UNCLAS	UL	44	19b. TELEPHONE NUMBER *(Include area code)*

Reset

Standard Form 298 (Rev. 8/98)
Prescribed by ANSI Std. Z39.18

TABLE OF CONTENTS

LIST OF FIGURES

SUMMARY

This technical report describes a computational research task performed to support continuing investigations into the electromagnetic behavior of photonic crystals. Simple dielectric vein structures are used to mimic the configuration of the photonic crystals found within the wings of the Green Hairstreak Butterfly, an insect noted for its use of photonic crystals for coloration. An earlier investigation employed a square dielectric vein structure to approximate these photonic crystals. In this case, the numerical model is improved. A rectangular vein structure is employed with two distinct values for the vein dielectric permittivity. The performance of the rectangular model is compared with that of the square model for both the Transverse Electric and Transverse Magnetic waves under mirror symmetry. The structure of attendant photonic bands is discussed.

1 INTRODUCTION

1.1 Background

The application of optics is well established in today's society and has been so since the days of Galileo's telescope and throughout the evolution of light microscopy. Optics, the physics of light, is a natural subdivision of the broader physics of electrodynamics and involves the in-depth study of electromagnetic waves propagating through various media. The propagation of electromagnetic waves can be controlled by manipulating the media containing the light. A good example of this idea is modern day optical fiber. An optical fiber is a specially designed waveguide that can propagate light over great distances with little or no losses. This type of optical device and attendant waveguide theory is discussed more thoroughly in Reference [1].

In the pages that follow, we turn our attention to a different type of optical device known as the Photonic Crystal (PC). PCs involve a higher level of complex light wave interactions than do optical fibers. In one, two or three dimensional space, these crystals are constructed by using a periodic distribution of dielectric material. A dielectric material is the matter carrying the light. Think of glass or even water as examples of dielectric media. Like optical fibers, PCs propagate light with very low losses.[2] The periodic distribution of dielectric material creates an array of interfaces in the crystal. At each interface, light waves both scatter and transmit electromagnetic energy. The superposition of incident and reflected waves, through the phenomenon of interference, may "block" the propagation of light of certain wavelengths. If light of all possible propagation directions (wave vectors) for a finite range of wavelengths (or frequencies) is blocked, the crystal exhibits a photonic band gap (PBG).[2] Band gaps can exert a strong effect over the colors of light propagated by a given photonic crystal. These crystals are purposeful and commonly exist in nature, particularly among insects, e.g., photonic crystals are found in certain butterfly wings and in the exo-skeletal chitin of certain species of beetle.[3] It is photonic crystals that are believed to cause the brilliant coloration found in many insects and birds.[4]

It is interesting to note that light (photons) interacting with the dielectric potential exhibit many of the same characteristics demonstrated by electrons encountering an atomic potential. Of course, the atomic potential is created by the distribution of electrical charge existing around atoms. By cleverly tailoring the atomic potential within a tiny silicon structure, one may construct a semi-conductor such as a transistor. This type of device is governed by solid state physics.[5] Because of the similar behavior of electromagnetic waves, we can apply many of the same techniques used in solid state physics to study photonic crystals. As it happens, mainly the differential operator and boundary conditions change when migrating from the study of electrons to photons. For electrons, we utilize the Schrödinger Equation while Maxwell's equations are applied for photons.[2]

1.2 Objectives

Section 2 begins with a concise exposition of the practical mathematics surrounding the solution of Maxwell's equations for light waves propagating in dielectric media. Our analysis is based exclusively in the frequency domain to permit the identification of optical frequencies and

modes. The system of equations is placed in time-harmonic form to derive the master eigenvalue problem. Vectors within the crystal lattice are then used to derive the reciprocal lattice in wave vector space. The associated Bloch wave vectors are used to place the master equation in Bloch form.

Section 3 contains a description of the square and rectangular crystal lattices of interest. The associated reciprocal lattices are presented, and the key points outlining the Brillouin zones for each reciprocal lattice are shown. The distribution of dielectric material is described for each 2D lattice.

Section 4 presents band diagrams (dispersion relations) for the square and rectangular lattices. Two different values of the relative dielectric permittivity are considered. Also, some of the mode shapes are plotted for the lower frequency Transverse Electric (TE) and Transverse Magnetic (TM) modes. We discuss specific differences between the optical modes for the square and rectangular lattices. Section 5 presents a summary for this report as well as a wrap-up of the conclusions.

2 THEORY

2.1 Maxwell's Equations

It is comforting to note, but perhaps a little less interesting, that even though many photonic crystals are small, we may treat light propagating within these crystals as electromagnetic waves instead of as a stream of photons. That is to say, we need not invoke quantum optics (yet).[6] As a result, this report will regard light propagation in PCs through the use of classic electromagnetism. In this context, the physics of time-dependent electromagnetic waves is governed by Maxwell's equations, a confluence of four separate partial differential equations derived over many years by researchers such as Coulomb, Gauss, Faraday and Ampere.[7] These equations were finally corrected for time dependency and assembled into a system by J.C. Maxwell.[8] The first equation in this system is Coulomb's (or Gauss') Law, i.e.,

$$\nabla \bullet \mathbf{D} = \rho \tag{1}$$

where $\mathbf{D}$, in the remainder of this work, is denoted as the displacement field, and ρ is the free charge density, a function defined in space. By assuming that space contains no free magnetic poles, we have that the second equation is

$$\nabla \bullet \mathbf{B} = 0 \tag{2}$$

(as it happens, free magnetic monopoles have never been discovered), where $\mathbf{B}$ is denoted the magnetic induction field. The third law is due to Faraday, i.e.,

$$\nabla \times \mathbf{E} + \frac{\partial \mathbf{B}}{\partial t} = 0 \tag{3}$$

where $\mathbf{E}$ is the electric field, and t is the time coordinate. The final equation is Maxwell's corrected form of Ampére's Law. One may recall, that in its original form, Ampére's "law" was not suitable for time dependent fields. The corrected equation is

$$\nabla \times \mathbf{H} - \frac{\partial \mathbf{D}}{\partial t} = \mathbf{J} \tag{4}$$

where $\mathbf{H}$ is denoted as the magnetic field; $\mathbf{J}$ is the current density function. These equations (1) through (4) are remarkable for a couple of different reasons. As a primary consideration, Maxwell's equations involve vector-valued quantities, the fields **B, E, H** and **D** as well as the current density vector **J**. Secondly, from the standpoint of mathematics, we have eight equations and the fifteen unknowns **B, E, H, D** and **J;** even if we assume that ρ is known, the system is not closed. Note that each vector component is a scalar unknown. The closure difficulty is resolved by invoking constitutive equations to relate **D** to **E** and **H** to **B**. We have that

$$\mathbf{D} = \varepsilon \mathbf{E} \tag{5}$$

where ε is the dielectric permittivity for the medium. For isotropic media, it may be expressed in terms of the vacuum permittivity (the permittivity of empty space ε_0), i.e.,

$$\varepsilon / \varepsilon_0 = 1 + \chi_e \quad \text{or} \quad \varepsilon = \varepsilon_0 \varepsilon_r \tag{6}$$

χ_e is the medium's electric susceptibility.[8] The term ε_r in equation (6) is denoted as the medium's relative dielectric permittivity. In some cases, this material property is frequency dependent. For anisotropic media, the relationship between the components of **D** and **E** is more complicated. According to the Bloembergen model, we have that

$$D_i / \varepsilon_0 = \varepsilon_{ij} E_j + \chi_{ijk} E_j E_k \tag{7}$$

where D_i and E_i represent the i^{th} components of the displacement and electric fields, respectively.[2] Instead of the simple constants used in (6), ε_{ij} and χ_{ijk} are tensor-based quantities that represent those cases where the point dielectric permittivity changes depending upon the direction of light propagation.

A similar constitutive relationship is employed to relate the magnetic and magnetic induction fields, i.e.,

$$\mathbf{B} = \mu \mathbf{H} \tag{8}$$

where μ is the magnetic permeability of the light propagating medium. This parameter is often measured with respect to the vacuum permeability μ_0.[8] Using a linear model for the permeability, we have

$$\mu = \mu_0 (1 + \chi_m) \tag{9}$$

in that χ_m is the magnetic susceptibility of the medium.[7] For anisotropic magnetic media, we may use the tensor-based form

$$H_i = \mu_{ij} B_j \tag{10}$$

a slightly different form of (8).[8] Normally, the magnetic susceptibility has a value near unity, but it may take on other values. The three equations represented by (10) require inversion to match the mathematical form of (8). Equations (5) and (8) provide six additional equations to help close the system. A potential formulation may be used to provide a final closure relation depending upon the choice of solution method for a particular problem.

2.2 Simplifying Maxwell's Equations

In this report, our goal is to solve Maxwell's equations for particular two-dimensional photonic crystals. The solution is performed in frequency space; both light frequencies and optical mode shapes are to be determined. In order to enable this analysis, Maxwell's equations are first cast in a simplified form. We begin by making a common assumption for light wave propagation problems, i.e., the medium contains no free electric charge ($\rho \equiv 0$) and no current density ($\mathbf{J} \equiv 0$). The dielectric permittivity is assumed to be independent of frequency and a function of position only; the magnetic permeability is set at the vacuum value. The space variables for the field are annotated by the position vector **r**. With these simplifications, the Maxwell equations can be written as

$$\nabla \bullet \mathbf{H}(\mathbf{r},t) = 0 \tag{11}$$

$$\nabla \bullet [\varepsilon(\mathbf{r})\mathbf{E}(\mathbf{r},t)] = 0 \tag{12}$$

$$\nabla \times \mathbf{E}(\mathbf{r},t) + \mu_0 \frac{\partial \mathbf{H}(\mathbf{r},t)}{\partial t} = 0 \tag{13}$$

$$\nabla \times \mathbf{H}(\mathbf{r},t) - \varepsilon_0 \varepsilon(\mathbf{r}) \frac{\partial \mathbf{E}(\mathbf{r},t)}{\partial t} = 0 \tag{14}$$

For efficiency of notation, the relative dielectric permittivity ε_r is now and hereafter denoted by $\varepsilon(\mathbf{r})$ in equations (12) and (14).[2] The next step is to address the time dependency of these equations.

As we stated earlier, our analysis is confined to frequency space, so the fields are assumed to be harmonic (or periodic) in time. Hence, they may be expressed in the form

$$\mathbf{H}(\mathbf{r},t) = \mathbf{H}(\mathbf{r},t)\exp(-i\omega t) \tag{15}$$

$$\mathbf{E}(\mathbf{r},t) = \mathbf{E}(\mathbf{r},t)\exp(-i\omega t) \tag{16}$$

where ω is the angular frequency for the light, and of course, i is the imaginary unit. Using Euler's formula, $\exp(-i\omega t) = \cos(\omega t) - i\sin(\omega t)$. When (15) and (16) are substituted into the divergence equations (11) and (12), we obtain

$$\nabla \bullet \mathbf{H}(\mathbf{r}) = 0 \tag{17}$$

$$\nabla \bullet [\varepsilon(\mathbf{r})\mathbf{E}(\mathbf{r})] = 0 \tag{18}$$

The Faraday (13) and Ampére (14) equations can be handled in a similar manner, yet an imaginary factor appears when the complex exponential is factored from these equations. The resulting equations are

$$\nabla \times \mathbf{E}(\mathbf{r}) - i\,\omega\,\mu_0\,\mathbf{H}(\mathbf{r}) = 0 \tag{19}$$

$$\nabla \times \mathbf{H}(\mathbf{r},t) + i\,\omega\,\varepsilon_0\,\varepsilon(\mathbf{r})\,\mathbf{E}(\mathbf{r},t) = 0 \tag{20}$$

The latter two equations are coupled, but by following Joannopoulos [2], they may be decoupled. Equation (20) is divided by the relative permittivity, and the curl of the result is taken to obtain the intermediate equation

$$\nabla \times \left(\frac{\nabla \times \mathbf{H}(\mathbf{r})}{\varepsilon(\mathbf{r})} \right) + i\,\omega\,\varepsilon_0\,\nabla \times \mathbf{E}(\mathbf{r}) = 0 \tag{21}$$

Next equation (19) is solved for $\nabla \times \mathbf{E}(\mathbf{r})$ and substituted into (21). The result is

$$\nabla \times \left(\frac{\nabla \times \mathbf{H}(\mathbf{r})}{\varepsilon(\mathbf{r})} \right) - \omega^2\,\varepsilon_0\,\mu_0\,\mathbf{H}(\mathbf{r}) = 0 \tag{22}$$

Equation (22), denoted as the master equation, is quite important; note that c^2 , the speed of light squared is the inverse of $\sqrt{\varepsilon_0\,\mu_0}$, so we have that

$$\nabla \times \left(\frac{\nabla \times \mathbf{H}(\mathbf{r})}{\varepsilon(\mathbf{r})} \right) = \left(\frac{\omega}{c} \right)^2 \mathbf{H}(\mathbf{r}) \tag{23}$$

The master equation consists of a linear differential form operating on the magnetic field and set equal to a constant times the magnetic field creating an eigenvalue problem with eigenvalue $(\omega/c)^2$ and eigenvector **H**(**r**). The linear differential form (or operator) is written as

$$\Theta = \nabla \times \left(\frac{1}{\varepsilon(\mathbf{r})} \nabla \times \right) \tag{24}$$

When **H**(r) has been determined, the electric field is obtained from (20) as

$$\mathbf{E}(\mathbf{r}) = \frac{i}{\omega\,\varepsilon_0\,\varepsilon(\mathbf{r})} \nabla \times \mathbf{H}(\mathbf{r}) \tag{25}$$

2.3 Frequency – Wave Vector Solution

The primary output of the analyses that follow is a numerical relationship between frequency (ω) and the wave vector $(\mathbf{k} = (k_x, k_y, k_z))$ for propagating light waves. This

relationship is often referred to as the dispersion relation. The wave vector magnitude $k = \| \mathbf{k} \|$ is simply the wavenumber $2\pi / \lambda$, where λ is the wavelength for the light. The wave vector implies a sense of direction to the wave. For an analysis in 2D or 3D, there is a locus of pertinent wave numbers revealed by the theory. For example, when considering a 2D problem at the plane of mirror symmetry, we can, without a loss of generality, assume that the crystal is uniform along the z axis with $k_z = 0$. As a result, light propagation is confined to the xy-plane with the attendant wave vector ($\mathbf{k} = (k_x, k_y, 0)$). It follows that the dispersion relation is a locus of the form

$$\omega = \omega(k_x, k_y) \tag{26}$$

where k_x and k_y vary, in the most general sense, between 0 and ∞. More specifically, we choose only the most pertinent wave vectors in the reciprocal plane, particularly those bordering the Brillouin zone.[2,9] To accomplish this task, we must express the magnetic field in Bloch form.

Bloch form is closely associated with the idea that our photonic crystal is composed of an array of dielectric material that is periodic (or repetitive) in some sense across the entirety of the crystal lattice. More specifically, we require the lattice to have discrete translational symmetry with a lattice constant vector $\mathbf{a}$.[2] Let the vector $\mathbf{R}$ be an integer multiple of the lattice constant vector, i.e.,

$$\mathbf{R} = n\mathbf{a} \tag{27}$$

Then values of the dielectric permittivity abide by the relationship

$$\varepsilon(\mathbf{r}) = \varepsilon(\mathbf{r} + \mathbf{R}) \tag{28}$$

for all possible integer values of n. Related to the geometric lattice in physical space is the reciprocal lattice cast in wave vector space. The reciprocal lattice vectors $\mathbf{b}_j$ are defined as follows.[10]

$$\mathbf{b}_j \bullet \mathbf{a}_i = 2\pi \delta_{ij} \tag{29}$$

Based upon this definition, the Bloch wave vector is defined in 3-space as

$$\mathbf{k} = k_1 \mathbf{b}_1 + k_2 \mathbf{b}_2 + k_3 \mathbf{b}_3 \tag{30}$$

Each wave vector (30) existing within the Brillouin zone (of the reciprocal lattice) identifies an eigenstate with angular frequency $\omega(\mathbf{k})$ for the operator (24).[2] The associated eigenvector (or eigenfunction) has the form

$$\mathbf{H}_{\mathbf{k}}(\mathbf{r}) = \exp(i\mathbf{k}\bullet\mathbf{r})\mathbf{u}_{\mathbf{k}}(\mathbf{r}) \tag{31}$$

In this eigenvector, $\mathbf{u}_k(\mathbf{r})$ is a periodic function defined on the physical lattice. We can find a partial differential equation for this function by substituting (31) into the master equation (23), i.e.,

$$\nabla\times\left[\frac{1}{\varepsilon(\mathbf{r})}\nabla\times\exp(i\mathbf{k}\bullet\mathbf{r})\mathbf{u}_{\mathbf{k}}(\mathbf{r})\right] = \left(\frac{\omega}{c}\right)^2\exp(i\mathbf{k}\bullet\mathbf{r})\mathbf{u}_{\mathbf{k}}(\mathbf{r}) \tag{32}$$

The term inside of the square brackets can be simplified by applying the vector identity

$$\nabla\times(f(\mathbf{r})\mathbf{g}) = f(\mathbf{r})\nabla\times\mathbf{g} + \nabla f(\mathbf{r})\times\mathbf{g} \tag{33}$$

Equation (33) requires $\nabla(\exp(i\mathbf{k}\bullet\mathbf{r}))$. This expression is derived as follows.

$$\begin{aligned}\nabla(\exp(i\mathbf{k}\bullet\mathbf{r})) = \frac{\partial}{\partial x_l}\exp(i\mathbf{k}\bullet\mathbf{r}) &= \exp(i\mathbf{k}\bullet\mathbf{r})\, i k_j \frac{\partial x_j}{\partial x_l} = \exp(i\mathbf{k}\bullet\mathbf{r})\, i k_j \delta_{jl} \\ &= i\mathbf{k}\exp(i\mathbf{k}\bullet\mathbf{r})\end{aligned} \tag{34}$$

By using (33) and (34) in (32), we obtain

$$\nabla\times\left[\frac{1}{\varepsilon(\mathbf{r})}\exp(i\mathbf{k}\bullet\mathbf{r})\{\nabla\times\mathbf{u}_{\mathbf{k}}(\mathbf{r}) + i\mathbf{k}\times\mathbf{u}_{\mathbf{k}}(\mathbf{r})\}\right] = \left(\frac{\omega}{c}\right)^2\exp(i\mathbf{k}\bullet\mathbf{r})\mathbf{u}_{\mathbf{k}}(\mathbf{r}) \tag{35}$$

Simplifying (35) further, we have that

$$\nabla\times\left[\frac{1}{\varepsilon(\mathbf{r})}\exp(i\mathbf{k}\bullet\mathbf{r})\{\nabla + i\mathbf{k}\}\times\mathbf{u}_{\mathbf{k}}(\mathbf{r})\right] = \left(\frac{\omega}{c}\right)^2\exp(i\mathbf{k}\bullet\mathbf{r})\mathbf{u}_{\mathbf{k}}(\mathbf{r}) \tag{36}$$

Now (33) is applied again to the square bracketed term with $f(\mathbf{r}) = \exp(i\mathbf{k}\bullet\mathbf{r})$ and $\mathbf{g} = 1/\varepsilon(\mathbf{r})(\nabla + i\mathbf{k})\mathbf{u}_{\mathbf{k}}(\mathbf{r})$. The result is

$$\begin{aligned}\exp(i\mathbf{k}\bullet\mathbf{r})\nabla\times\left[\frac{(\nabla + i\mathbf{k})}{\varepsilon(\mathbf{r})}\times\mathbf{u}_{\mathbf{k}}(\mathbf{r})\right] + \nabla\exp(i\mathbf{k}\bullet\mathbf{r})\times\left[\frac{(\nabla + i\mathbf{k})}{\varepsilon(\mathbf{r})}\times\mathbf{u}_{\mathbf{k}}(\mathbf{r})\right] \\ = \left(\frac{\omega}{c}\right)^2\exp(i\mathbf{k}\bullet\mathbf{r})\mathbf{u}_{\mathbf{k}}(\mathbf{r})\end{aligned} \tag{37}$$

Continued simplification with the use of (34) yields a new eigenvalue equation

$$\left\{(\nabla + i\mathbf{k}) \times \frac{(\nabla + i\mathbf{k})}{\varepsilon(\mathbf{r})} \times\right\} \mathbf{u}_{\mathbf{k}}(\mathbf{r}) = \left(\frac{\omega}{c}\right)^2 \mathbf{u}_{\mathbf{k}}(\mathbf{r}) \tag{38}$$

The operator $\{\bullet\}$ in (38) is also Hermitian, yet it is not used alone.[2] We can derive a fundamental constraint equation for transverse waves by substituting the Bloch form (31) into (17). With the use of the vector identity

$$\nabla \times (f(\mathbf{r})\mathbf{g}) = f(\mathbf{r})\nabla \bullet \mathbf{g} + \nabla f(\mathbf{r}) \bullet \mathbf{g} \tag{39}$$

we obtain the result

$$(\nabla + i\mathbf{k}) \bullet \mathbf{u}_{\mathbf{k}}(\mathbf{r}) = 0 \tag{40}$$

Equation (38) subject to the constraint (40) and the periodicity condition

$$\mathbf{u}_{\mathbf{k}}(\mathbf{r}) = \mathbf{u}_{\mathbf{k}}(\mathbf{r} + \mathbf{R}) \tag{41}$$

can be solved for the frequencies and eigenfunctions describing light propagation in the photonic crystal.[11] Solving this set of equations on a dielectric lattice is the purpose of the MIT Photonic Bands (MPB) computer program applied to produce the results shown later in this report.

3 LATTICE DESCRIPTIONS

The goal of the present work is to present and contrast optical modes for a set of square and rectangular dielectric vein structures. These 2D photonic crystals (uniform in the third Cartesian direction) are selected for study because of their likeness to a simplified view of the photonic crystals found in the wings of *Callophrys rubi*, the green hairstreak butterfly.[3] An electron micrograph of a part of the wing is shown in Figure 1. While the computational lattices shown below do not approach the level of complexity of the actual butterfly wing, some of the larger geometric structures may be captured by an elementary numerical model.

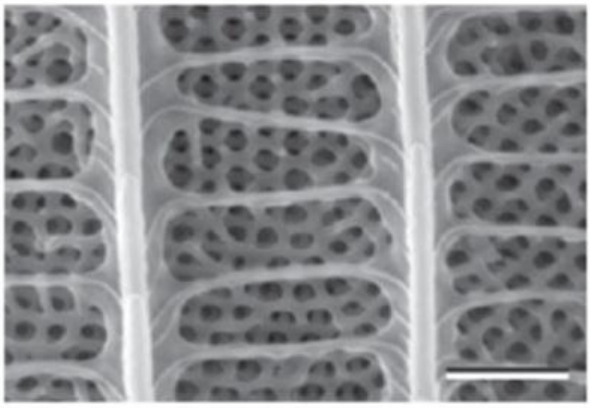

Figure 1. Electron micrograph of photonic crystals located in the wings of *Callophyrs rubi*[3]

3.1 Square Dielectric Vein Lattice

The square dielectric vein lattice is a relatively simple 2D geometric object.[2] The lattice is comprised of thin horizontal and vertical veins of dielectric material separating square regions filled with air. Figure 2 contains a representative picture of the lattice with the dielectric veins (uniform thickness) colored black; air filled regions are white.

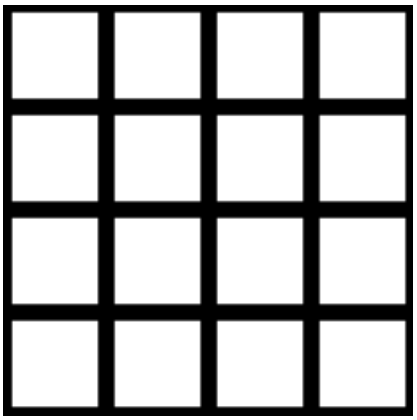

Figure 2. Diagram of the Square Dielectric Vein Lattice. Unit cell is repeated three times in the horizontal and vertical directions

For this lattice, the physical lattice vectors are:

$$\begin{aligned}\mathbf{a}_1 &= a(1,0)\\ \mathbf{a}_2 &= a(0,1)\end{aligned} \tag{42}$$

Recall that Maxwell's equation are scale invariant, so the lattice constant "a" in (42) is an arbitrary scaling factor (units of distance) that may be used to establish a lattice of any desired size as long as we do not violate the minimum scale for the electromagnetic wave model. Equation (29) may be used to show that the reciprocal lattice vectors are:

$$\begin{aligned}\mathbf{b}_1 &= \frac{2\pi}{a}(1,0)\\ \mathbf{b}_2 &= \frac{2\pi}{a}(0,1)\end{aligned} \tag{43}$$

The dielectric veins have width of $0.165a$ (appropriately scaled with the lattice constant). Figure 3 contains a plot of the unit cell for this physical lattice. In this figure, the dielectric material is

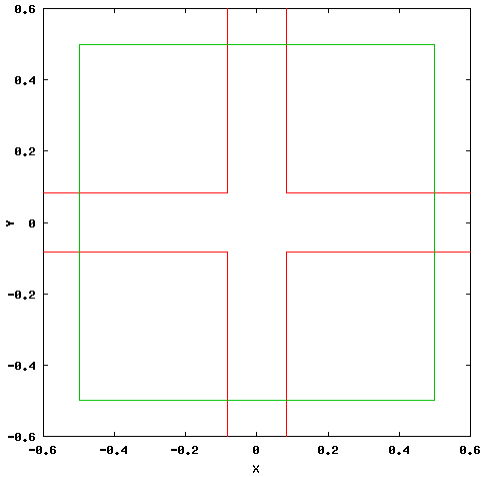

Figure 3. Unit cell for the square dielectric vein lattice. Dielectric boundaries are shown in red. Unit cell boundary is shown in green. All lengths have the dimensions of the lattice constant *a*

outlined with the color red and has a cruciform shape centered at the figure's center. The boundary for the unit cell is delineated by the green line. The calculations conducted with the use of this lattice geometry are dimensionless, yet the x and y coordinates naturally inherit the dimensions of the lattice constant a. This report considers two values for the relative dielectric permittivity. The baseline case sets $\varepsilon = 8.9$ to provide a strong jump in the electric field at the dielectric-air interface. The baseline is selected to establish a dielectric/air permittivity difference of nearly 10:1. The second case sets $\varepsilon = 1.52$ somewhat closer to a value for chitin, a material commonly found in butterfly wings. In future studies, ε is to be raised to 2.4, a common value for chitin.[12]

The reciprocal of the square dielectric vein lattice can be easily produced by spanning the reciprocal lattice vectors. A wave vector $\mathbf{k} = (k_x, k_y)$ in the reciprocal lattice is given by the formula

$$\mathbf{k} = l\mathbf{b}_1 + m\mathbf{b}_2 , \quad l, m = 0, \pm 1, \pm 2, \ldots \tag{44}$$

More specifically,

$$\mathbf{k} = \frac{2\pi}{a}(l, m), \quad l, m = 0, \pm 1, \pm 2, \ldots \tag{45}$$

For equation (45), dimensions are only assigned by the lattice constant a ; if the lattice constant is assigned specific length dimensions, **k** then possesses dimensions of a wave number. The reciprocal lattice for the square dielectric vein configuration is shown in Figure 4.

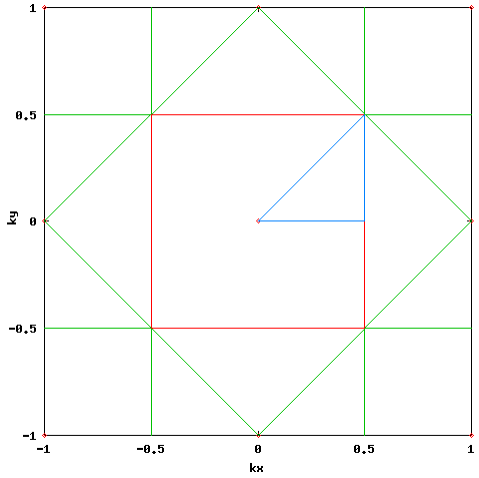

Figure 4. Reciprocal lattice for the square dielectric vein configuration. Axes are delineated with dimensions of wave number. The red points shown in the diagram are produced by the mapping (45). The red square outlines the Brillouin zone for this lattice. The blue lines outline the irreducible Brillouin zone. Key points are defined at the vertices of the irreducible zone

Figure 4 is constructed by summing integer multiples of the reciprocal lattice vectors. The Brillouin Zone (BZ) (more appropriately titled as the first Brillouin zone) is produced by the procedures described in References 2 and 9. In short, it is minimum area figure that is bounded by parallel rays constructed through the center points of line segments extending between reciprocal lattice points. The irreducible Brillouin zone (IBZ), shown outlined in blue, is the minimum area locus that can be used to map the solution in the rest of the BZ by a series of simple rotations and translations.[2] The points at the vertices of the IBZ are key locations for calculation of the frequency space solution.

3.2 Rectangular Dielectric Vein Lattice

The principal photonic crystal of interest in this report is the rectangular dielectric vein lattice. The square lattice discussed in the preceding section is actually a special case of the

rectangular lattice. The rectangular lattice is of interest since its configuration is more like the array of chitin shown in Figure 1. A picture of the rectangular dielectric vein lattice is shown in Figure 5. Three multiples of the unit cell are shown in each direction.

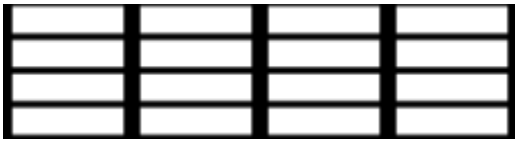

Figure 5. Diagram of the rectangular dielectric vein lattice. Unit cell is repeated three times in the horizontal and vertical directions. Note the difference between vertical and horizontal vein widths

In Figure 5, the black color represents dielectric material while air is represented by white. For this photonic crystal, the width of vertical veins is $0.13157a$; horizontal veins have a width of $0.052631a$ where a is the lattice constant. The air gap width and height are $0.86842a$ and $0.21052a$, respectively. These parameters are chosen to match the aspect ratio of the chitin-air cells shown in Figure 1. Two parameters are required to describe the physical lattice vectors for this configuration. These vectors are

$$\begin{aligned} \mathbf{a}_1 &= a(1,0) \\ \mathbf{a}_2 &= a(0,\theta) \end{aligned} \tag{46}$$

In this case, θ is chosen as 0.26315. The unit cell for the physical lattice is shown in Figure 6.

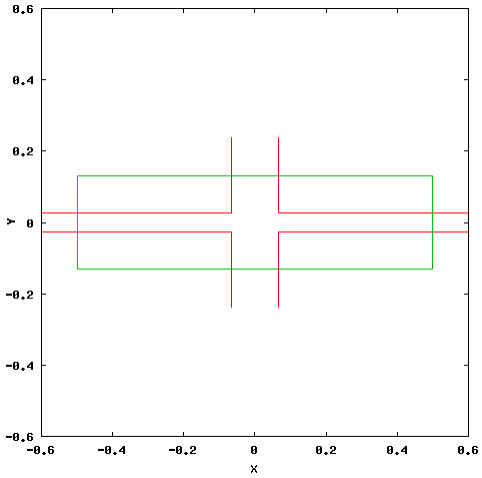

Figure 6. Unit cell for the rectangular dielectric vein lattice. Dielectric boundaries are shown in red. Unit cell boundary is shown in green. All lengths have the dimensions of the lattice constant *a*

The reciprocal lattice vectors are derived as

$$\mathbf{b}_1 = \frac{2\pi}{a}(1,0)$$
$$\mathbf{b}_2 = \frac{2\pi}{a}(0,1/\theta) \tag{47}$$

Wave vectors in the reciprocal lattice are defined as in equation (44) with the specific result

$$\mathbf{k} = \frac{2\pi}{a}\left(l, \frac{m}{\theta}\right), \quad l,m = 0,\pm 1,\pm 2,\ldots \tag{48}$$

A diagram of the reciprocal lattice for the rectangular vein structure is shown in Figure 7. One

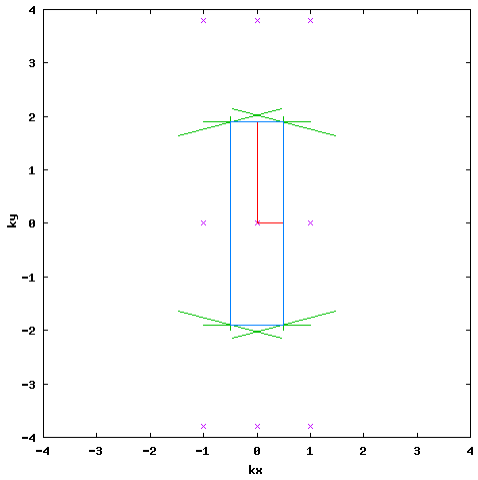

Figure 7. Reciprocal lattice for the rectangular dielectric vein configuration. Axes are delineated with dimensions of wave number. The magenta points shown in the diagram are produced by the mapping (45). The blue square outlines the Brillouin zone for this lattice. The red lines outline the irreducible Brillouin zone. Key points are defined at the vertices of the irreducible Brillouin zone

may notice that the IBZ is rectangular in shape for this lattice.[9] For the square lattice, the IBZ is triangular. A possible explanation for this result is that the rectangular lattice lacks a symmetry occurring in the square lattice (at the $k_x = k_y$ line). This result is very interesting and begs future investigation concerning symmetry operations in the Brillouin zone. The lattice geometries described in this and the preceding sections summarize the input used for calculating the electromagnetic behavior of the square and rectangular 2D photonic crystals. Again, as with the square lattice, our choice of relative dielectric permittivity values remains the same.

4 RESULTS

The electrical field results (dispersion relations and mode shapes) shown below have been calculated by using the MIT Photonic Bands (MPB) computer code developed by the Joannopoulos *Ab Initio* Physics Group at the Massachusetts Institute of Technology.[11] The theory behind the frequency domain solution methods applied within MPB is briefly discussed in Section 2 of this report. In this section, we present the results predicted by MPB for the 2D photonic crystal configurations presented in the preceding section.

4.1 Transverse Electric (TE) Wave Propagation at $\varepsilon = 8.90$

Electromagnetic wave solutions for the square and rectangular vein dielectric lattices have been calculated at a relative dielectric permittivity (ε) value of 8.90. Figure 8 contains the dispersion relations (band diagrams) for TE wave propagation at $\varepsilon = 8.9$ for both lattices.

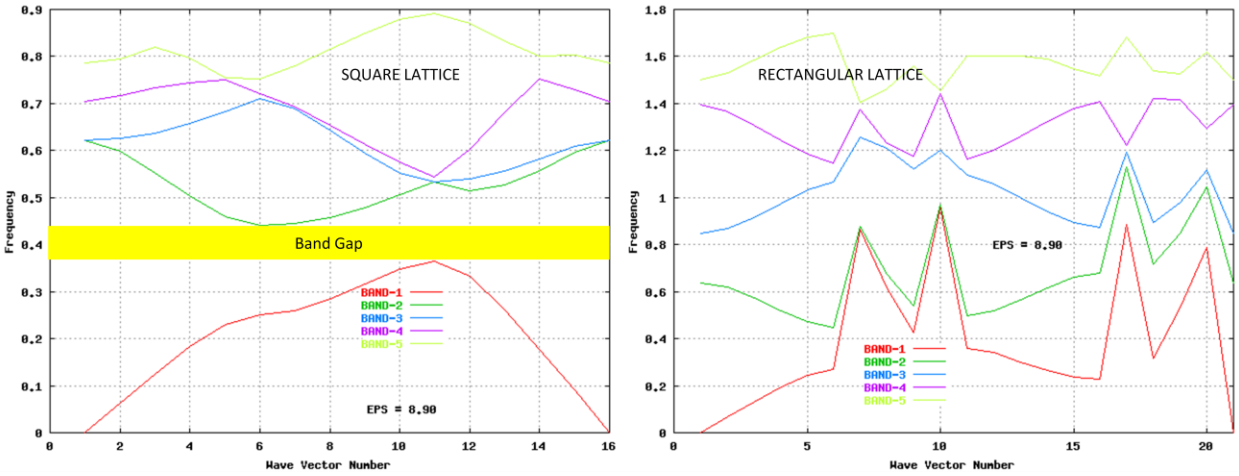

Figure 8. Dispersion relations for transverse electric (TE) wave propagation in the square and rectangular dielectric vein lattices at relative permittivity 8.9. The dispersion relation for the square lattice is shown in the left plot while the plot for rectangular lattice is presented on the right. The notation wave vector number is used to indicate the location of the wave vector on the boundary of the irreducible Brillouin zone. Only the first five eigenmodes are displayed

Within the square lattice, a band gap is evident for TE waves. The rectangular lattice exhibits no band gaps. It is interesting to compare 2D contour plots of the eigenmode shapes for these cases. We begin by examining the TE mode shapes for $\varepsilon = 8.9$, a baseline case useful for comparison. Recall that for the TE mode, the electric field is confined to the *xy*-plane; its *z* component is zero. The associated magnetic field is aligned with the *z* axis. All of the mode shape plots that follow are computed at wave vectors (k-points) $\mathbf{k} = 2\pi/a$ (0.5, 0.5, 0) for the square lattice and at $\mathbf{k} = 2\pi/a$ (0.5, 1.9, 0) for the rectangular lattice. These k-points are identified in Figure 8 with wave vector number 11 for both lattices. For the fundamental frequency, Figure 9 contains the plots of the real part of E_x for each lattice. Note that both lattices are graphed on plots of the same size even though their aspect ratios differ. Doing so facilitates a side-by-side comparison of the electric field components. As is evident in Figure 9, the difference in this field component is quite large when moving between the square lattice (left) and the rectangular lattice (right). In fact, E_x is many times stronger in the rectangular lattice than it is in the square lattice. The mode

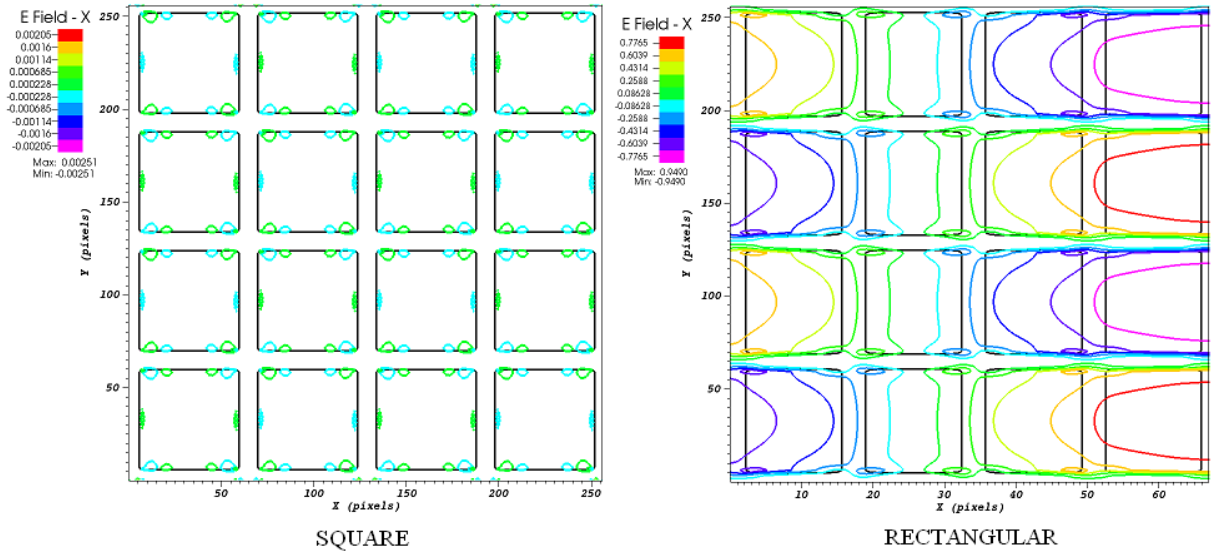

Figure 9. Real part of E_x for the fundamental frequency computed at (left) k-point (wave vector) $2\pi/a$ (0.5,0.5,0) in the square lattice and at (right) k-point $2\pi/a$ (0.5,1.9,0) in the rectangular lattice. Vein dielectric permittivity 8.90

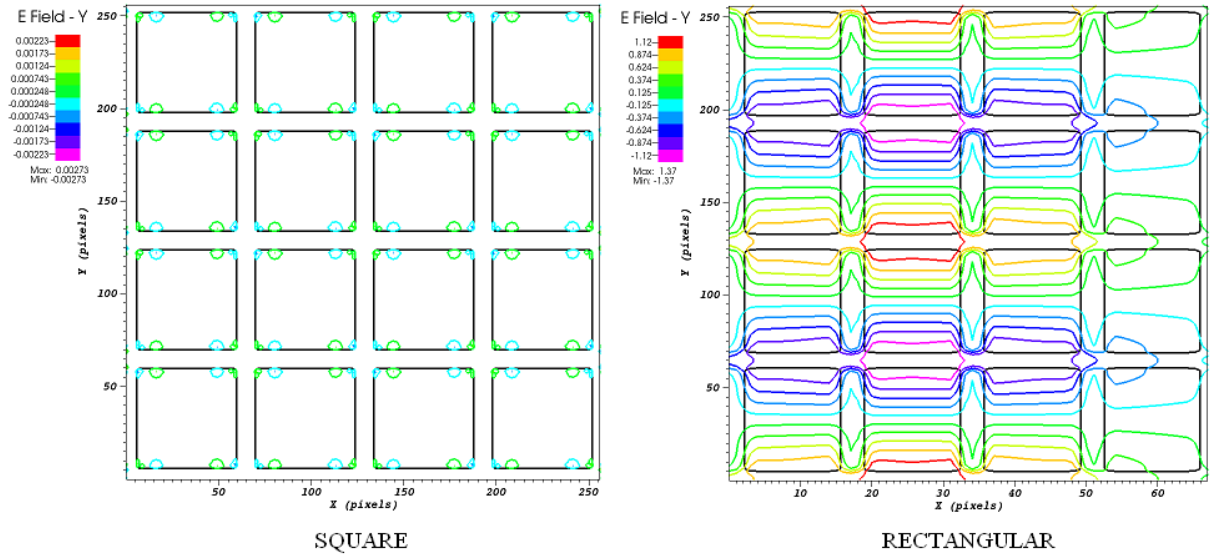

Figure 10. Real part of E_y for the fundamental frequency computed at (left) k-point (wave vector) $2\pi/a$ (0.5,0.5,0) in the square lattice and at (right) k-point $2\pi/a$ (0.5,1.9,0) in the rectangular lattice. Vein dielectric permittivity 8.90

shape is more widespread on the rectangular lattice than on the square lattice. On the square lattice, variations in E_x are mostly confined to the vein junctions (or spots [2]). At these junctions, E_x exhibits quadrupolar variation. For the rectangular lattice, E_x is significantly compressed elongating it in the x direction. It is also interesting to see that nodes are located along the horizontal veins. Also, the periodic variation in E_x extends well beyond the lattice shown. In fact, one needs to extend the lattice over eight unit cells in order to see the field variation. The real part of the y component of the electric field E_y is shown in Figure 10. In this

case, field component oscillations for the square lattice are still centered around the vein junctions, but possess a dipolar character. Nodes are situated within the air space throughout the lattice. For the rectangular lattice, the field has greater extent with periodicity extending beyond the section of the lattice shown. The extent of the field can be observed if more cells are plotted. The locus of field nodes occurs along horizontal lines through the center of the air space. The peaks in E_y are also out of phase with respect to the peaks in E_x.

We continue our examination of TE mode propagation by considering the next higher frequency for both lattices. Figure 11 contains plots of the real part of E_x at the same k-points selected for the square and rectangular lattices. It is evident that the field behavior is different in

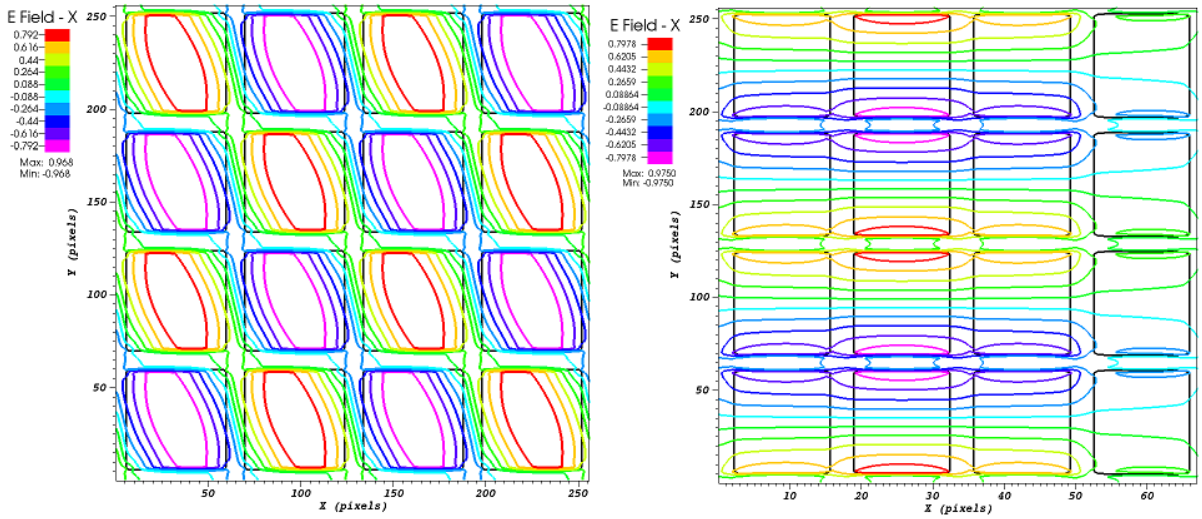

SQUARE RECTANGULAR

Figure 11. Real part of E_x for the second frequency computed at (left) k-point (wave vector) $2\pi/a$ (0.5,0.5,0) in the square lattice and at (right) k-point $2\pi/a$ (0.5,1.9,0) in the rectangular lattice. Vein dielectric permittivity 8.90

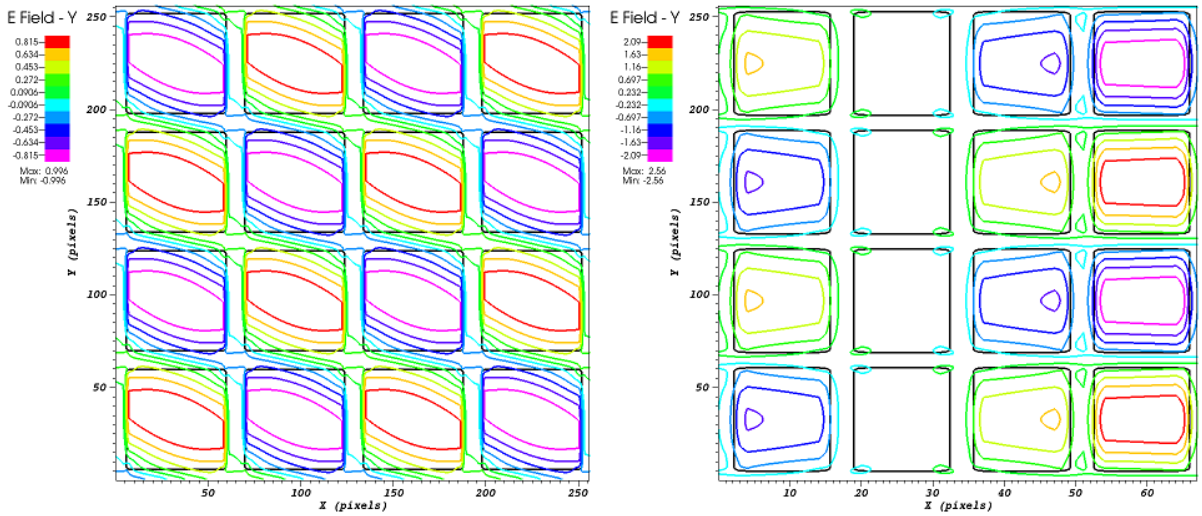

SQUARE RECTANGULAR

Figure 12. Real part of E_y for the second frequency computed at (left) k-point (wave vector) $2\pi/a$ (0.5,0.5,0) in the square lattice and at (right) k-point $2\pi/a$ (0.5,1.9,0) in the rectangular lattice. Vein dielectric permittivity 8.90

this case, especially for the square lattice. Figure 12 contains the associated contour plots for E_y. For the square lattice at this the next to lowest frequency, the differences in electric field behavior are very pronounced. For the fundamental frequency, the field activity is concentrated near the vein lattice spots (vein junctions) with some dipolar activity on the vertical veins. Since the veins possess high relative dielectric permittivity $\varepsilon = 8.9$, we expect that the field will concentrate near the veins.[2] For the second frequency we see different behavior for the square lattice. E_x nows concentrates in the air space between the veins, i.e., in the *air band*. The field variation also indicates dipolar variation (horizontal for E_x and vertical for E_y). Why does the electric field change so dramatically? The answer is simple. Figure 8 clearly shows that a band gap exists on the square lattice for the TE mode between the fundamental and second frequencies.

Differences calculated on the rectangular lattice when transitioning between the two frequencies are not as pronounced. On this lattice, E_x still has nodes located along horizontal lines in the air space. The highest magnitude values of E_x lie on the horizontal veins. E_y is the stronger component of the two. This behavior may be caused by the fact that horizontal dielectric veins are closer together and tend to concentrate field lines nearby. On the other hand, the mode shape (or field distribution) for E_y changes to a greater degree. The peaks and troughs in this field component clearly occur in the air spaces, and the component varies more slowly in the horizontal direction than in the vertical direction. The phase difference between E_x and E_y remains and possesses roughly the same magnitude as for the fundamental mode. Of course, the second frequency is very close to the fundamental for the wave vector in question (at wave vector number 11 in Figure 8). Hence, the modes behave in a similar manner.

Continuing with our investigation, we turn our attention to the third frequency exhibited at the k-points in question. Contours of the real part of the *x* component of the electric field are shown in Figure 13 for both the square and rectangular lattices. For this case, field variation is

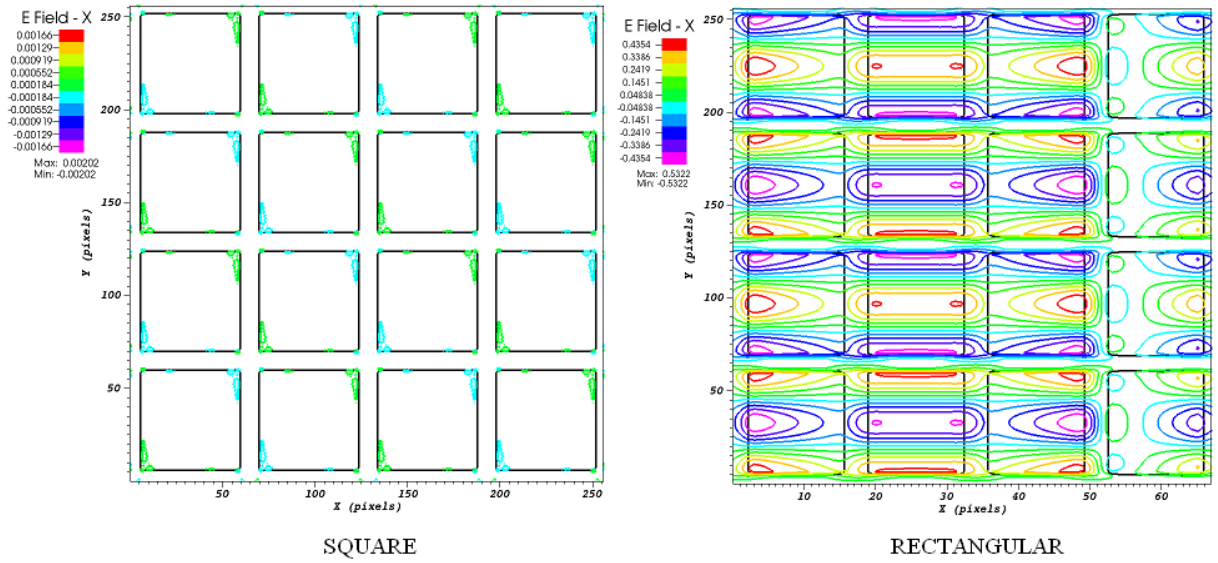

SQUARE RECTANGULAR

Figure 13. Real part of E_x for the third frequency computed at (left) k-point (wave vector) $2\pi/a$ (0.5,0.5,0) in the square lattice and at (right) k-point $2\pi/a$ (0.5,1.9,0) in the rectangular lattice. Vein dielectric permittivity 8.90

again centered at spots in the square lattice. For the rectangular lattice, variation in $\Re(E_x)$ is similar to that exhibited at the second frequency. Extrema exist at loci along horizontal veins and at the centers of the air spaces. Figure 14 contains the corresponding plots for $\Re(E_y)$. On the

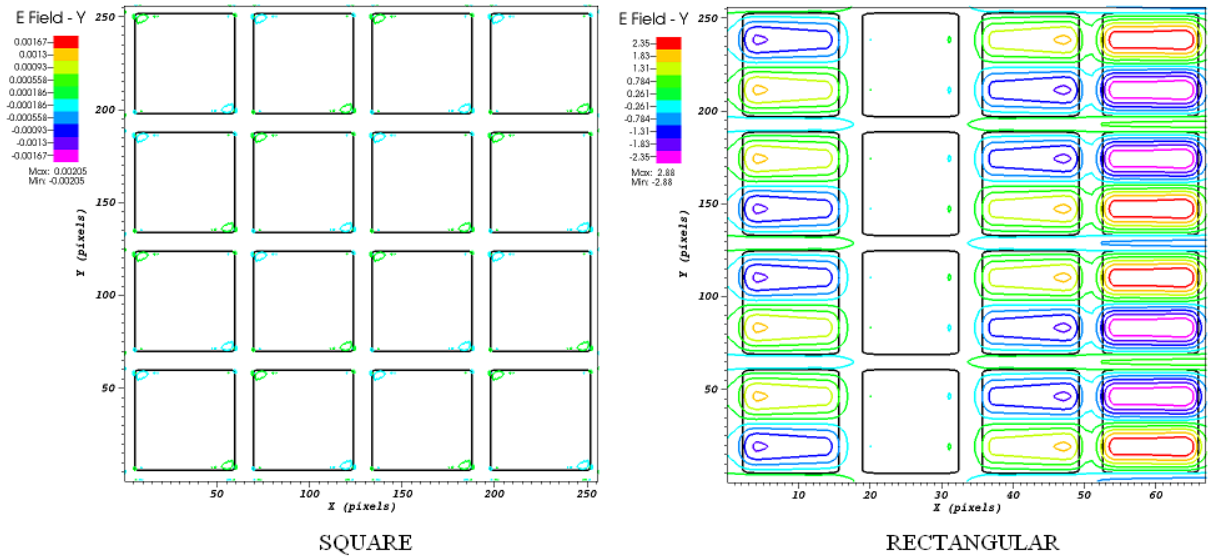

SQUARE RECTANGULAR

Figure 14. Real part of E_y for the third frequency computed at (left) k-point (wave vector) $2\pi/a$ (0.5,0.5,0) in the square lattice and at (right) k-point $2\pi/a$ (0.5,1.9,0) in the rectangular lattice. Vein dielectric permittivity 8.90

square lattice, the variation of E_y is similar to that of E_x; these field oscillations are concentrated again around the vein junctions (spots) and possess some of the characteristics of quadrupoles. The variation of E_x at the same frequency is more dipolar. On the rectangular lattice, the field oscillations are still predominantly oriented in the horizontal direction. The field nodes exist horizontally along veins and at the air gap centers. The periodic nature of the field extends well beyond the section of the lattice shown, and the phase difference is still exhibited between *x* and *y* electric field components.

4.2 Transverse Electric (TE) Wave Propagation at $\varepsilon = 1.52$

In this section of the report, we repeat the analyses perform in Section 4.1 now for the relative permittivity of $\varepsilon = 1.52$. The dispersion relations for the square and rectangular dielectric vein lattices are shown in Figure 15. The first characteristic of the band diagrams shown is that neither lattice possesses a bad gap. This result is anticipated since the difference between the relative permittivity (index of refraction squared) for the dielectric and air is so small. Secondly, the band diagram for the rectangular lattice is sharply peaked and jagged at several wave vector numbers, far more so than for the square lattice. This jaggedness is very pronounced at the lower frequencies for a wide range of wave vectors. The rectangular lattice also reaches, for a given eigenmode, a higher range of frequencies than does the square lattice. These regions in the dispersion relation graph correspond to the edges of the Brillouin zone where k_y changes with k_x is fixed. In the crystal lattice, this region corresponds to the edges that change in the *y* direction. The higher frequencies encountered in this region may be explained as

follows. In order to fit a fixed number of wavelengths within this distance, a comparatively shorter wavelength and thus a higher frequency must be used (when compared to the square

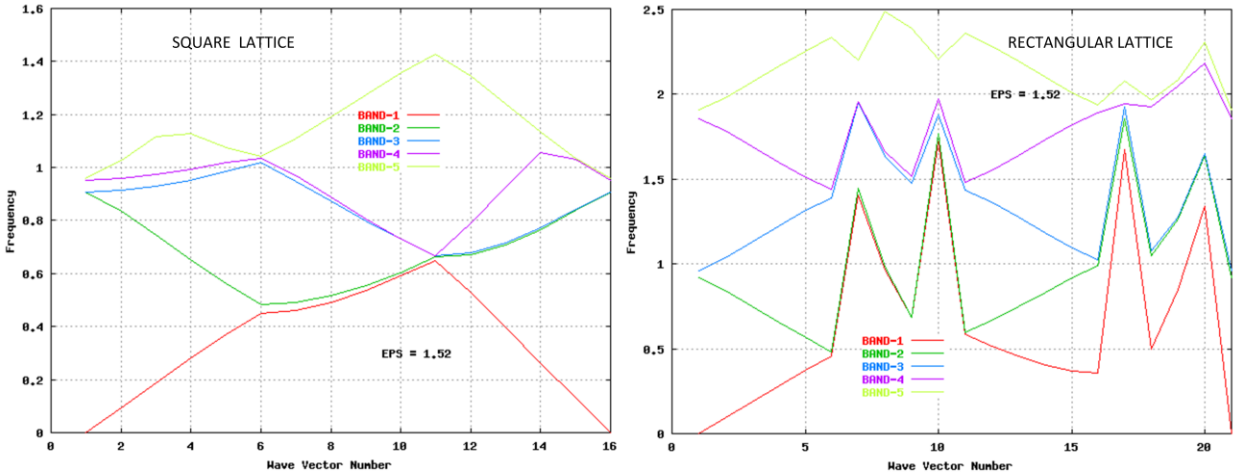

Figure 15. Dispersion relations for transverse electric (TE) wave propagation in the square and rectangular dielectric vein lattices at relative permittivity 1.52. The dispersion relation for the square lattice is shown in the left plot while the plot for rectangular lattice is presented on the right. We notation wave vector number is used to indicate the location of the wave vector on the boundary of the irreducible Brillouin zone. Only the first five eigenmodes are displayed.

lattice). When examining the mode shapes for this case, we use the same k-points specified in the preceding section.

Figure 16 contains TE mode shapes for the x component of the electric field E_x at the fundamental frequency calculated at wave vector number 11 for both the square (left) and rectangular (right) lattices. For the square lattice, E_x clearly exhibits dipolar behavior with the field nodes aligned along the vertical veins. Adjacent horizontal lattice tiers alternate in phase.

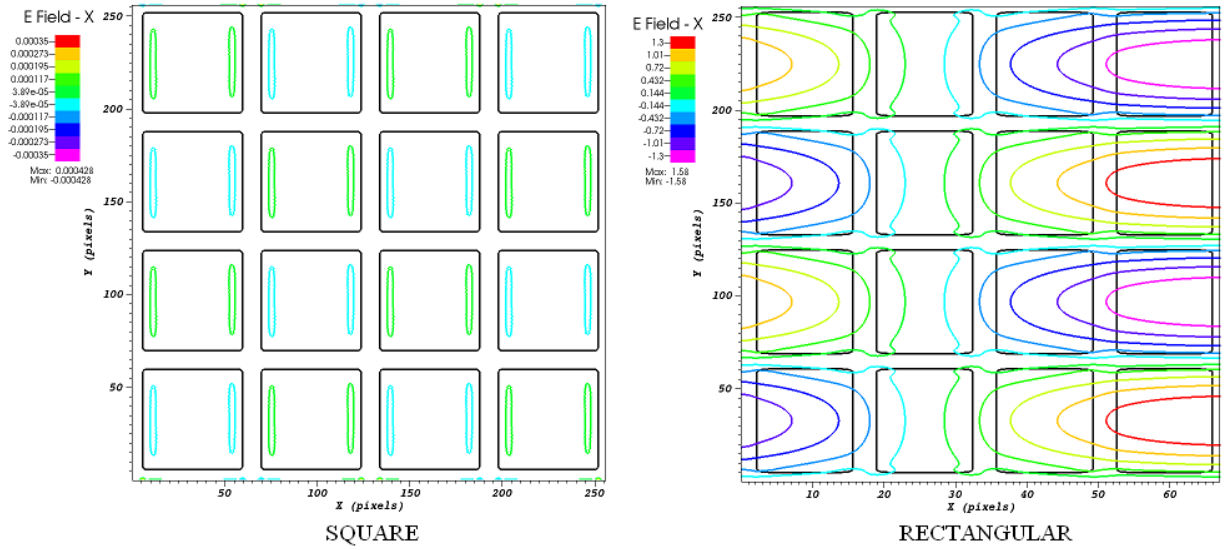

Figure 16. Real part of E_x for the fundamental frequency computed at (left) k-point (wave vector) $2\pi/a$ (0.5,0.5,0) in the square lattice and at (right) k-point $2\pi/a$ (0.5,1.9,0) in the rectangular lattice. Vein dielectric permittivity 1.52

On the rectangular lattice, E_x shares the same dipolar character, but the field oscillations are more extensive on the lattice. The nodes are oriented along vertical aligned loci located at the centers of air gaps. These vertical loci are spaced apart at a periodicity (in terms of unit cells) exceeding the extent lattice segment shown in the figure. The magnitude of the variations in E_x for the

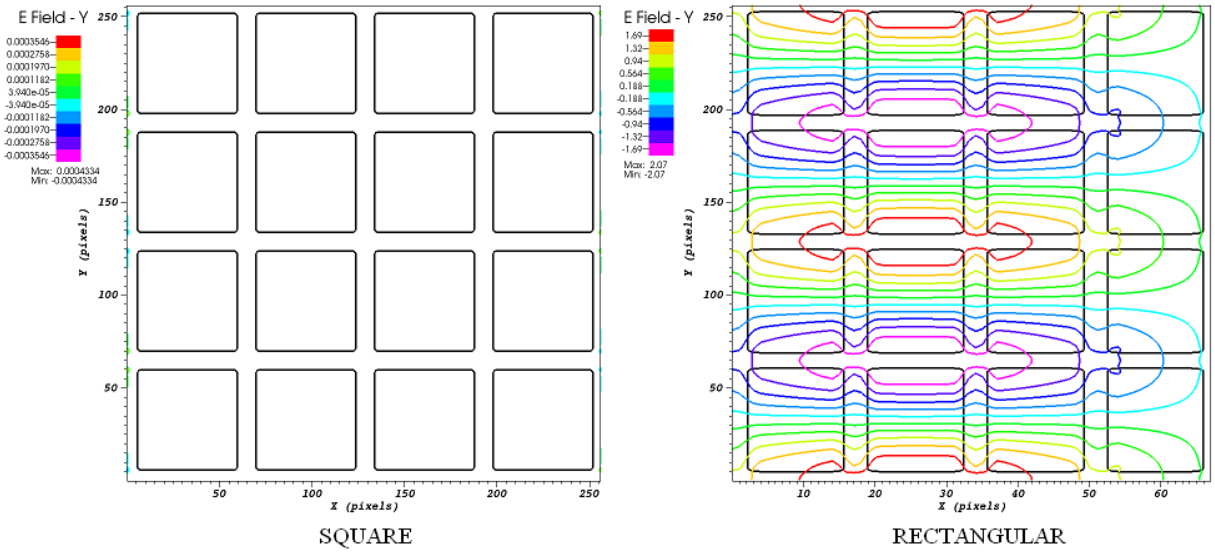

Figure 17. Real part of E_y for the fundamental frequency computed at (left) k-point (wave vector) $2\pi/a$ (0.5,0.5,0) in the square lattice and at (right) k-point $2\pi/a$ (0.5,1.9,0) in the rectangular lattice. Vein dielectric permittivity 1.52

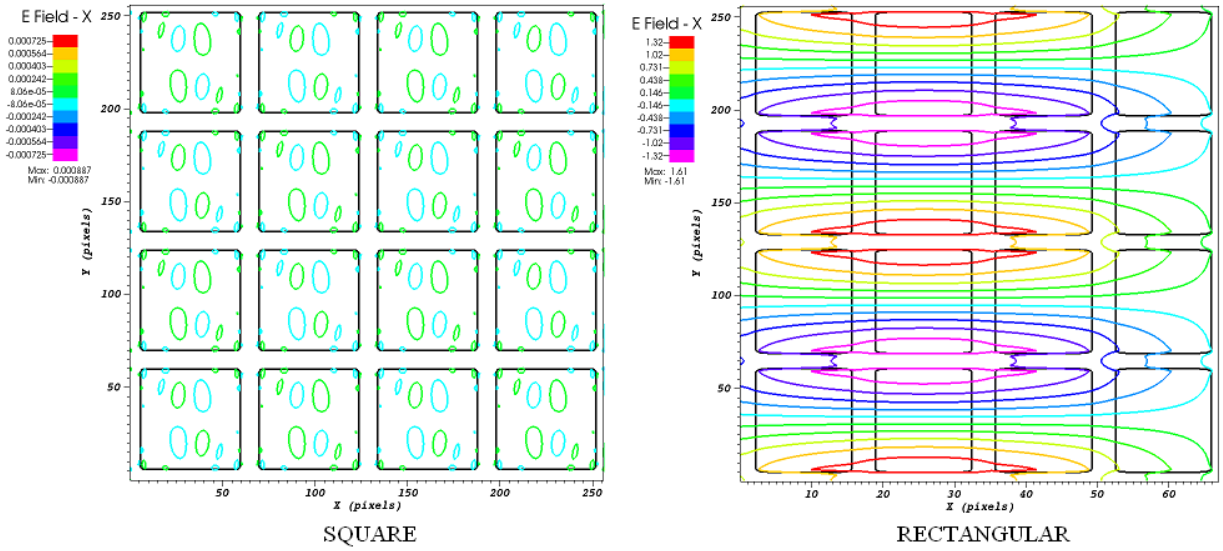

Figure 18. Real part of E_x for the second frequency computed at (left) k-point (wave vector) $2\pi/a$ (0.5,0.5,0) in the square lattice and at (right) k-point (0.5,1.9,0) in the rectangular lattice. Vein dielectric permittivity 1.52

rectangular lattice are considerably larger than those calculated for the square lattice. The peak values in E_x are located at air gap centers. Figures 17 present the *y* component of the electric field for the fundamental frequency. This component's behavior is interesting because on the square lattice, it possesses almost no detectable magnitude. Hence, the electric field for the square

lattice is fully aligned with the x axis. On the other hand, the rectangular lattice E_y has its peak magnitudes centered along the horizontal veins with nodes situated along horizontal loci located at the air gap centers. The phase difference for the x and y components persists as shown in the previous cases. The structure of the electric field for the rectangular lattice exhibits a great deal of commonality for different frequencies. Consider the behavior of the electric field for the two lattices at the second modal frequency. E_x for the square lattice, shown in Figure 18, exhibits

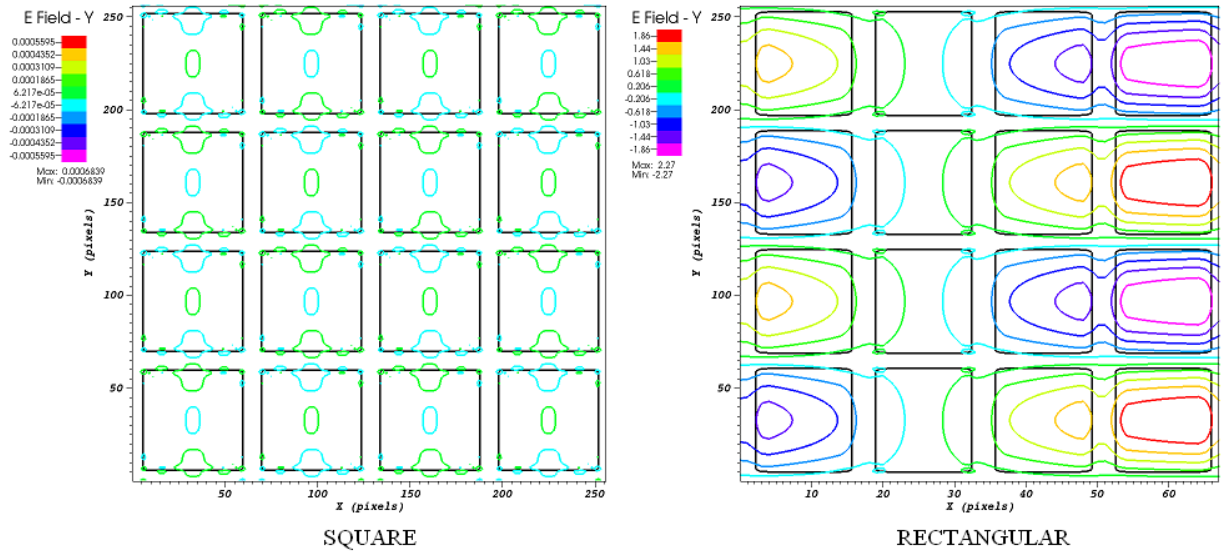

Figure 19. Real part of E_y for the second modal frequency computed at (left) k-point (wave vector) $2\pi/a$ (0.5,0.5,0) in the square lattice and at (right) k-point $2\pi/a$ (0.5,1.9,0) in the rectangular lattice. Vein dielectric permittivity 1.52

fluctuations centered at the vein junctions (spots) and within the air gaps. A quadrupole-like variation is observed within the air gaps while between vein spots, a dipolar fluctuations exists. E_x for the rectangular lattice exhibits the same dipolar variation with the field peaks located along the horizontal veins. The horizontal node loci are found at the air gap centers. Figure 19 contains the plots of E_y for the second modal frequency. The square lattice's field is dominated by dipolar variations that recur throughout the crystal. These variations are centered on horizontal veins with an additional lobe of the fluctuation located at the air gap center. For the rectangular lattice, E_y still possesses a dipolar shape except peak field magnitudes are located along horizontal loci located at air gap centers. The field contours do exhibit some higher order characteristics like multiple local maxima and minima. We continue with our investigation by considering electric field behavior at the third modal frequency.

Figure 20 contains plots of Ex for the third modal frequency computed for the square and rectangular lattice structures ( ). The square lattice is characterized by the presence of monopoles centered at the vein spots. The rectangular lattice exhibits a more complicated system of dipoles aligned with the horizontal veins. The peaks are centered on both the horizontal veins and at the air gap centers. The maximum positive and negative peaks alternate from vein to air gap when scanning in the y direction along the lattice. The plots for Ey are provide in Figure 21. In this case, the square lattice is characterized by the presence of more monopoles, this time located at the air gap centers. The positive and negative peak magnitudes alternate between adjacent monopoles. In this case, nodes form loci along the veins. The rectangular lattice clearly

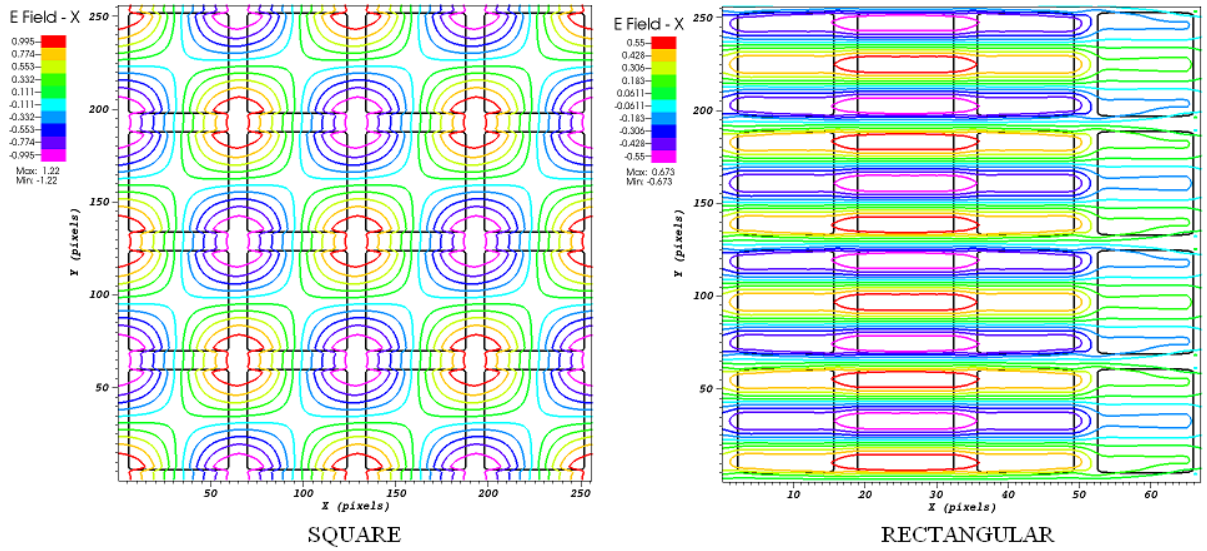

Figure 20. Real part of E_x for the third modal frequency computed at (left) k-point (wave vector) $2\pi/a$ (0.5,0.5,0) in the square lattice and at (right) k-point $2\pi/a$ (0.5,1.9,0) in the rectangular lattice. Vein dielectric permittivity 1.52

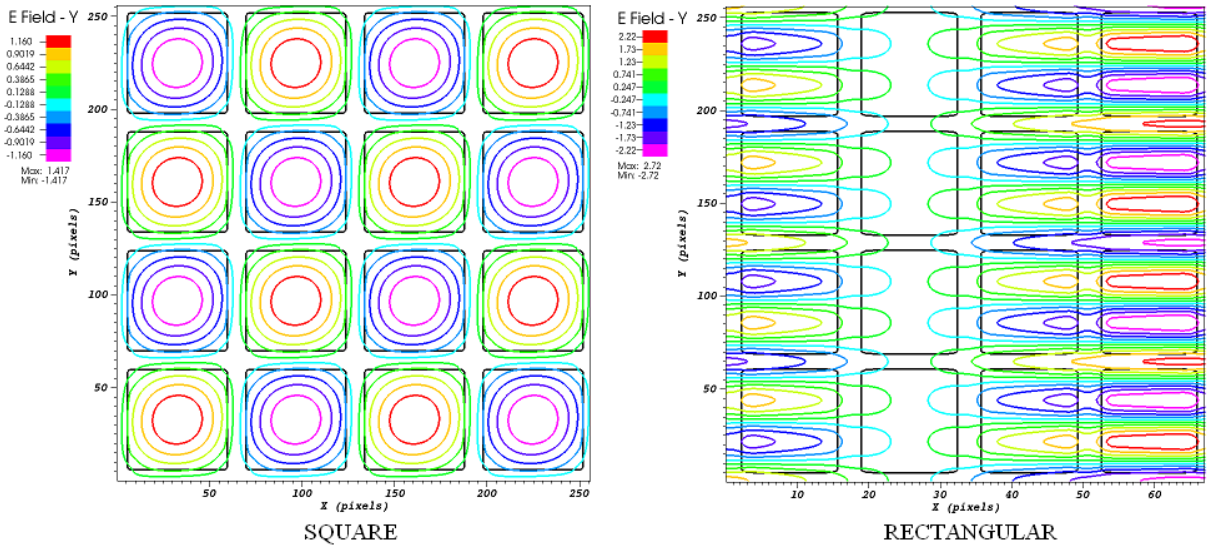

Figure 21. Real part of E_y for the third modal frequency computed at (left) k-point (wave vector) $2\pi/a$ (0.5,0.5,0) in the square lattice and at (right) k-point $2\pi/a$ (0.5,1.9,0) in the rectangular lattice. Vein dielectric permittivity 1.52

exhibits more complex dipole behavior with peak values existing along horizontal veins and at air gap centers. In this case, a cycle requires 2/3 of a unit cell (vertically) for completion. As in the previous cases, there is an outstanding phase difference between E_x and E_y. It seems evident that the field behavior on the rectangular lattice is governed, to a great degree, by field compression created by the reduced spacing between horizontal veins. The spacing between horizontal veins is roughly 26% of the spacing between vertical veins.

4.3 Transverse Magnetic (TM) Wave Propagation at $\varepsilon = 8.90$

Our discussion of electromagnetic wave propagation on the two test lattices is incomplete without including a discussion of TM wave propagation. Recall that since the magnetic field components are confined to the *xy*-plane, there is only one electric field component, E_z, aligned in the *z* direction. Band diagrams have been prepared for TM propagation. Figure 22 contains these diagrams for the test lattices at $\varepsilon = 8.90$. The square lattice possesses a small band gap of

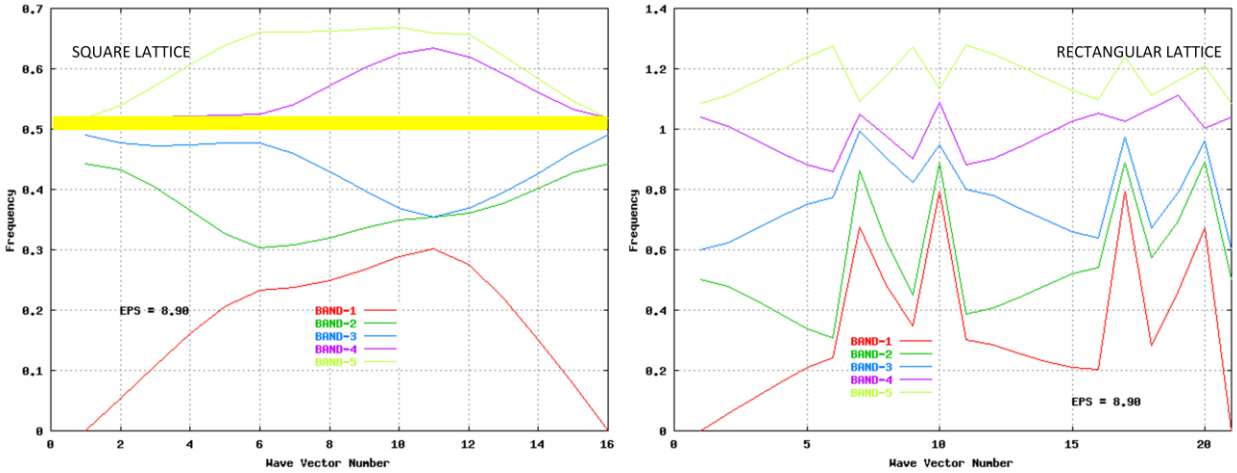

Figure 22. Dispersion relations for transverse magnetic (TM) wave propagation in the square and rectangular dielectric vein lattices at relative permittivity 8.90. The dispersion relation for the square lattice is shown in the left plot while the plot for rectangular lattice is presented on the right. The notation wave vector number is used to indicate the location of the wave vector on the boundary of the irreducible Brillouin zone. Only the first five eigenmodes are displayed.

width 5.3% between bands 3 and 4. This gap is indicated by the yellow bar shown in Figure 22. The MPB computer code predicts two other band gaps, but these gaps are so small, their existence is questionable, i.e., they spuriously result because of numerics. The rectangular lattice contains no band gaps, but for larger dielectric permittivity values, one may form between modal frequencies four and five. The rectangular plot is characteristically jagged as are its predecessors for the TE propagation mode. We can now present the TM mode shapes.

At the fundamental frequencies, mode shapes for E_z are compared in Figure 23 for the two lattices. The square lattice is dominated by an array of monopoles, alternating in sense and centered at the vein spots. The rectangular lattice possesses dipole characteristics with peak values lying along horizontal veins. The nodes fall in two regions. The first is located along horizontal lines of air gap centers. The second region lies along vertical lines of gap centers; the periodicity for these loci extend outside of the section of the lattice shown. The peak magnitudes of E_z differ by less than a factor of three. Figure 24 contains plots of the real part of E_z for the second modal frequency. In this case, the square lattice is characterized by four-lobed wave structures centered at the vein spots. The polarity of these structures alternates between adjacent spots. Nodes exist at the air gap centers and at vein midpoints. The magnitude of these fluctuations is quite small. The rectangular lattice retains dipolar behavior with a horizontal periodicity that extends beyond the lattice segment shown. The peak field magnitudes for the rectangular lattice exceed those for the corresponding square lattice mode. In the *y* direction, peaks in E_z alternate between air gap centers making for distinct *y*-oriented dipolar wave

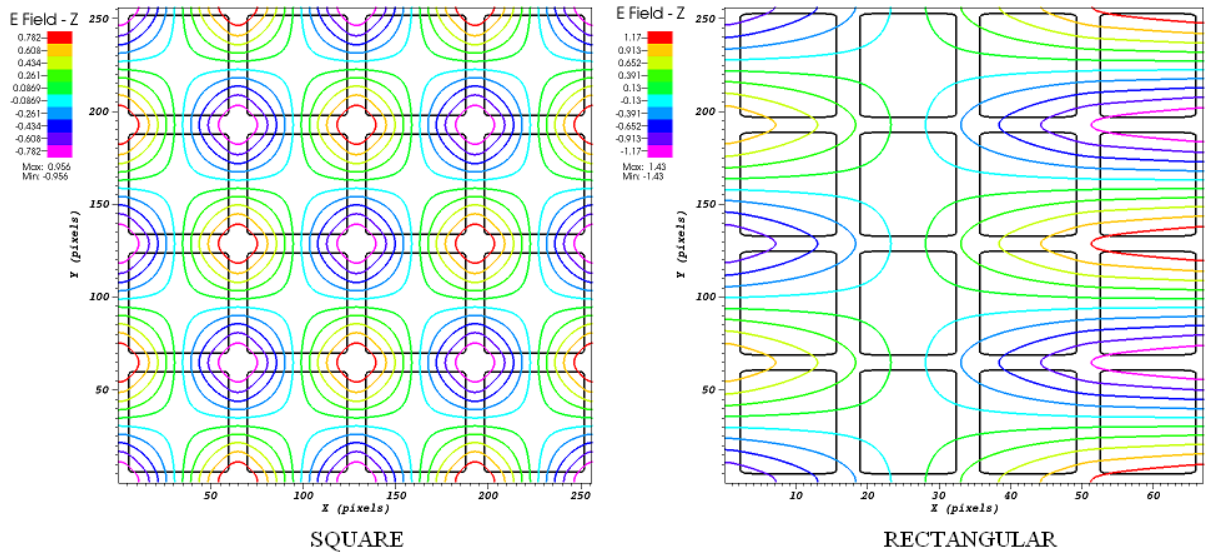

Figure 23. Real part of E_z for the fundamental TM mode computed at (left) k-point (wave vector) $2\pi/a$ (0.5,0.5,0) in the square lattice and at (right) k-point $2\pi/a$ (0.5,1.9,0) in the rectangular lattice. Vein dielectric permittivity 8.90

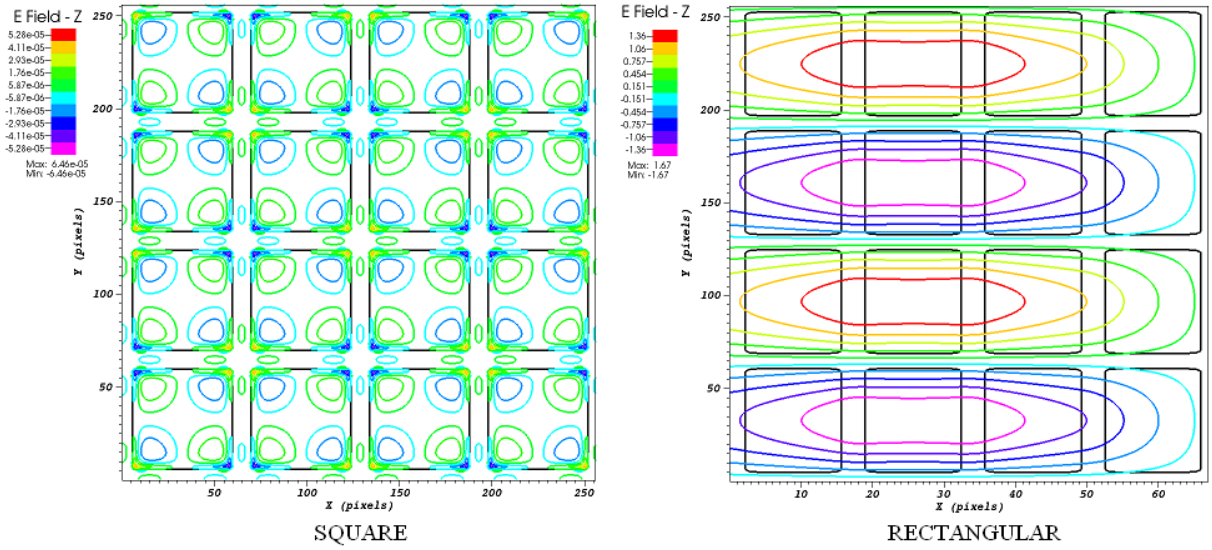

Figure 24. Real part of E_z for the TM mode at the second modal frequency computed at (left) k-point (wave vector) $2\pi/a$ (0.5,0.5,0) in the square lattice and at (right) k-point $2\pi/a$ (0.5,1.9,0) in the rectangular lattice. Vein dielectric permittivity 8.90

structures. Note that here is a clear phase difference between the first two rectangular modes. Mode plots for the third frequency are shown in Figure 25.

For the third modal frequency, the square lattice is dominated by an array of dipoles oriented in the *x* direction. The magnitude of the associated fluctuations is quite small with respect to the fundamental mode. The dipoles are centered within the air gaps; their senses alternate from those in adjacent cells. On the other hand, E_z in the rectangular lattice is composed

of more complicated dipoles oriented in the *y* direction. There is also a periodicity cast in the *x* direction, yet it extends beyond the segment of the lattice shown. The peak magnitudes are centered along the vertically oriented veins. The nodes are located also along these veins but occur at the air gap center. The peaks are juxtaposed to sides of the center making for an interesting wave form. This effect is a sign of higher order modal behavior. Of course, there are also lines of vertically oriented nodes as indicated at the right side of the rectangular lattice plot. This behavior is contrasted with that occurring for $\varepsilon = 1.52$ in the next section.

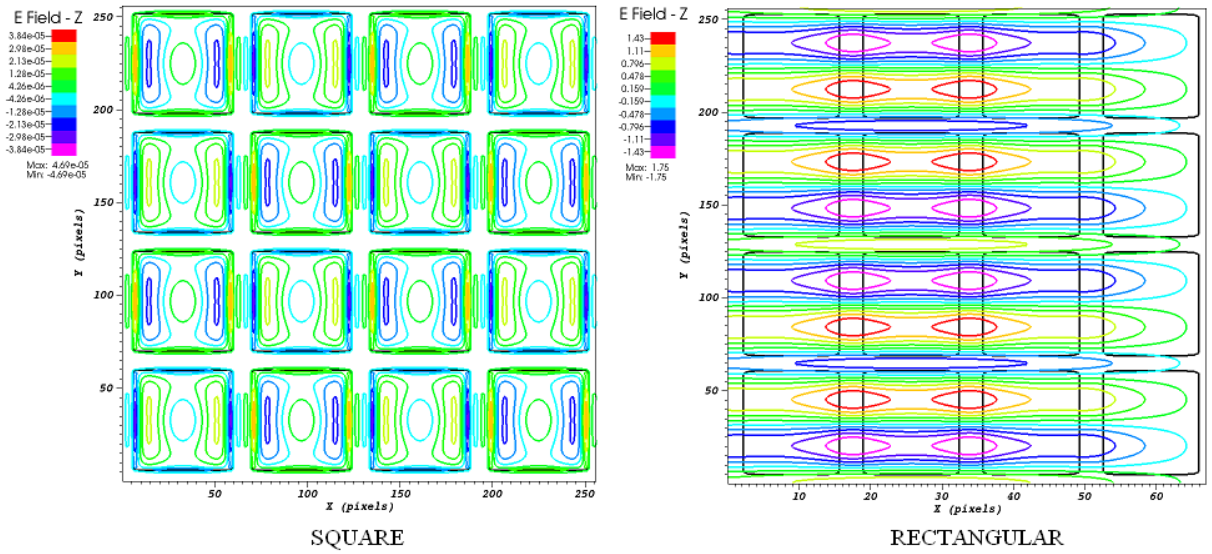

Figure 25. Real part of E_z for the TM mode at the third modal frequency computed at (left) k-point (wave vector) $2\pi/a$ (0.5,0.5,0) in the square lattice and at (right) k-point $2\pi/a$ (0.5,1.9,0) in the rectangular lattice. Vein dielectric permittivity 8.90

4.4 Transverse Magnetic (TM) Wave Propagation at $\varepsilon = 1.52$

TM electromagnetic wave propagation has been analyzed for the two test lattices with the index of refraction set to 1.52 in the dielectric veins. Band diagrams for the lattices are provided in Figure 26. In this case, no band gaps are observed in either lattice. The rectangular lattice does have the jagged appearance that we encountered in preceding section. We continue with a brief examination of the electric field mode shapes. Figure 27 contains plots for Ez mode shapes at the fundamental frequencies for both the square and rectangular lattices. The square lattice is dominated by monopoles centered at the vein spots. The rectangular lattice is characterized by dipoles oriented in the y direction. The peak field distributions are centered on the horizontal dielectric veins. There is also a secondary periodicity in the x direction that extends beyond the lattice segment shown. The field magnitudes differ by less than a factor of two between the two lattices at the fundamental frequencies. In Figure 28, the modal shapes for Ez are plotted. The square lattice is dominated by a complicated mode shape with nodes distributed along the veins. As previously encountered, the rectangular lattice is dominated by dipoles oriented in the y direction, but with a long wave periodicity in the *x* direction. In this case, the rectangular

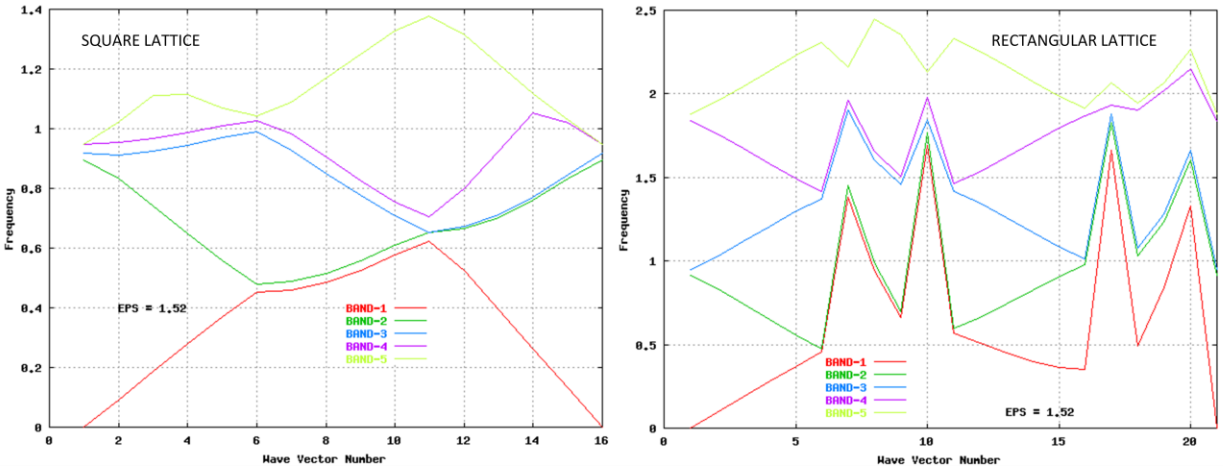

Figure 26. Dispersion relations for transverse magnetic (TM) wave propagation in the square and rectangular dielectric vein lattices at relative permittivity 1.52. The dispersion relation for the square lattice is shown in the left plot while the plot for rectangular lattice is presented on the right. The notation wave vector number is used to indicate the location of the wave vector on the boundary of the irreducible Brillouin zone. Only the first five eigenmodes are displayed.

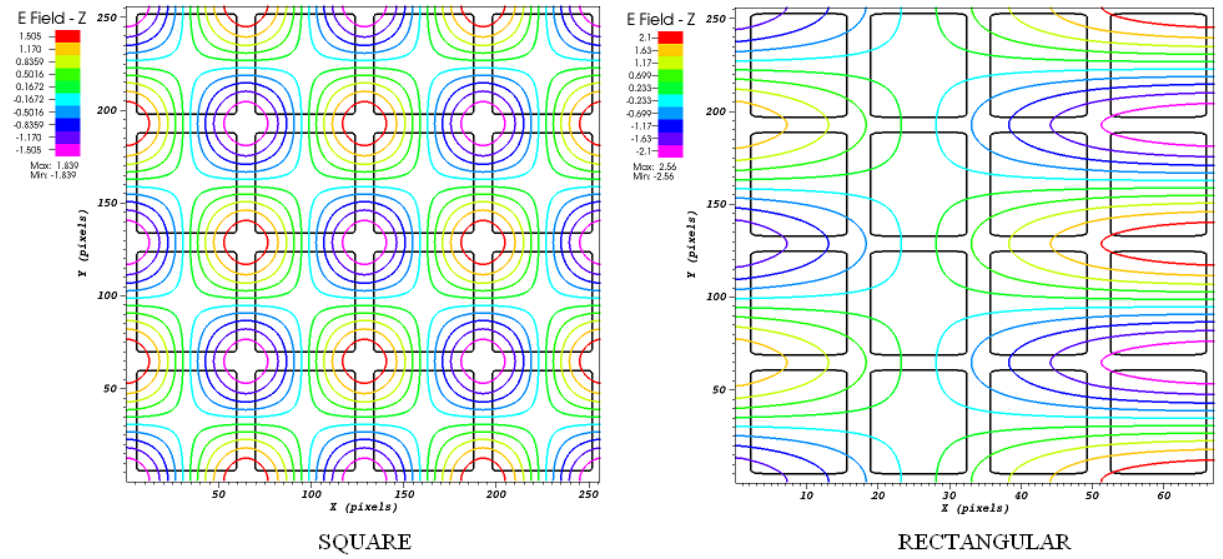

Figure 27. Real part of E_z for the fundamental TM mode computed at (left) k-point (wave vector) $2\pi/a$ (0.5,0.5,0) in the square lattice and at (right) k-point $2\pi/a$ (0.5,1.9,0) in the rectangular lattice. Vein dielectric permittivity 1.52

lattice's field magnitude exceeds the magnitude on the square lattice. Figure 29 contains the contours for the real part of E_z at frequencies for the third mode. This electric field component again has a very compact appearance on the lattice. Field oscillations are centered at the vein spots, but the magnitudes, at least with respect to the fundamental, are very small. The sense of the field reverses at alternating spots. In some sense, the field behaves in a dipolar manner, but the fluctuations are complex. On the other hand, the rectangular field has complicated dipolar characteristics with a primary orientation in the *y* direction. Peaks appear on the horizontal veins

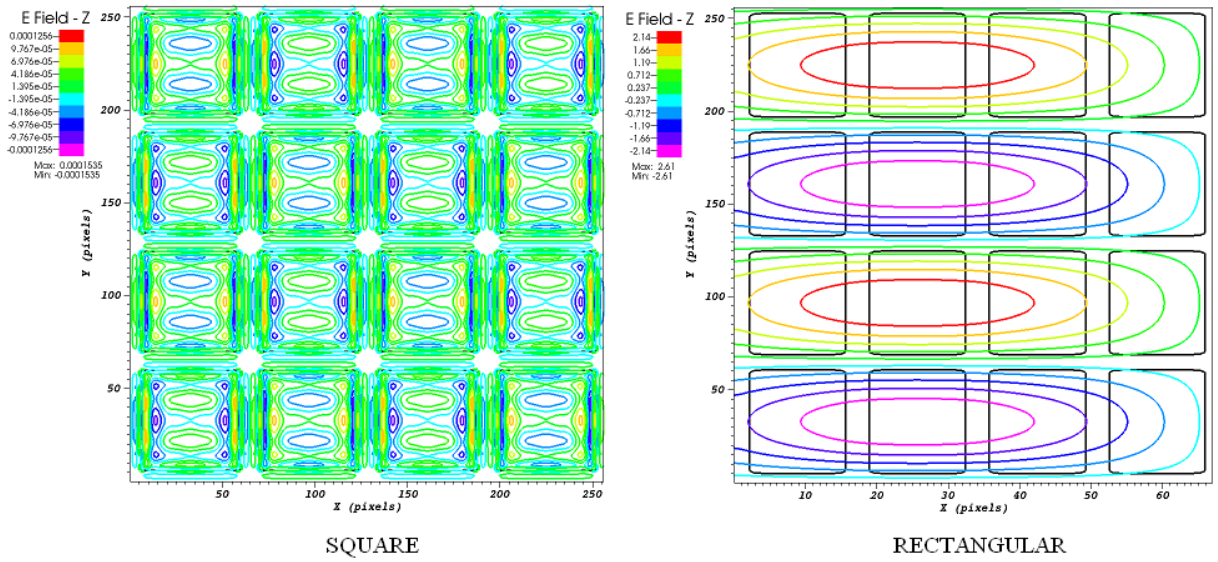

Figure 28. Real part of E_z for the TM mode at the second modal frequency computed at (left) k-point (wave vector) $2\pi/a$ (0.5,0.5,0) in the square lattice and at (right) k-point $2\pi/a$ (0.5,1.9,0) in the rectangular lattice. Vein dielectric permittivity 1.52

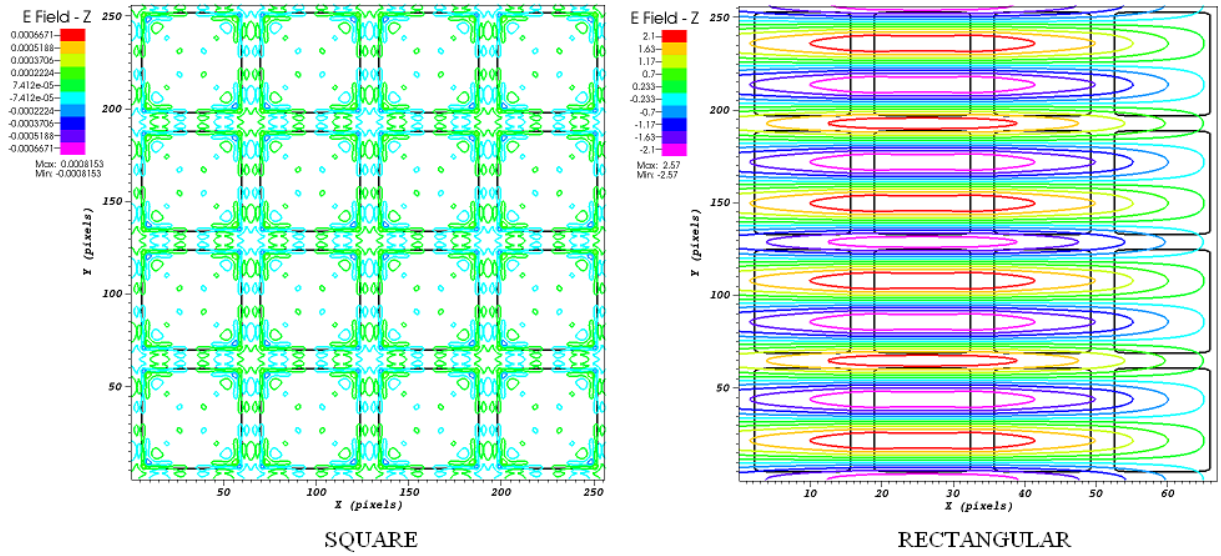

Figure 29. Real part of E_z for the TM mode at the third modal frequency computed at (left) k-point (wave vector) $2\pi/a$ (0.5,0.5,0) in the square lattice and at (right) k-point $2\pi/a$ (0.5,1.9,0) in the rectangular lattice. Vein dielectric permittivity 1.52

and at every third of the air gap. Of course, there is a long wave periodicity that extends in the *x* direction outside of the lattice segment shown. A significant investment of time can be required to fully examine and understand the implications of both TE and TM modal solutions. It is also important to note that we have only presented the shapes for three distinct frequencies associated with each of these modes. Obviously, there are many other modes. Instead of exploring higher order modes, it is instructive to turn our attention to interpreting the impact on light coloration associated with some of the modes detailed above.

4.5 Comparing Results for the Two Lattices

In preceding section, we have discussed a modal analysis of electromagnetic wave propagation for square and rectangular 2D crystal lattices. Our interest now lies in studying how differently light propagates on the rectangular lattice than on the square lattice. For high relative dielectric permittivity values, the square lattice possesses band gaps. Since the rectangular unit cell geometry is "closer" in shape to the photonic crystal mentioned in Section 3, one may ask if band gaps can appear for this lattice, especially for the relative dielectric permittivity of chitin, a value quite near unity. The square lattice's field exhibits highly uniform mode shapes when sampled at the so-called M k-point $2\pi/a$ (0.5.0.5.0). The electric field fluctuations are usually centered on each lattice spot, air gap center or at the midpoint of the dielectric vein. There are phase differences between the *x* and *y* components of the field lattice, but the phase difference is the width of one unit cell. This behavior is echoed for the square lattice at the lower value of $\varepsilon = 1.52$, yet in this case, no band gaps exist. Band gaps are usually created when the differences in ε are high across the lattice since the field concentrates in regions of high ε.[2] At this reduced dielectric value, the differences are too small to generate band gaps.

Our interest is to see if similar behavior occurs for the rectangular lattice, even at the higher dielectric value. The calculations show that the rectangular field is very different. Although the field fluctuations are periodic on the rectangular lattice, the periodicity in the *x* direction is manifested over a distance of several unit cells. That is to say, for the square lattice, the period for a complete field oscillation is no more than two cells. For the rectangular case, the period in the *y* direction is usually two cells, but in the *x* direction, a period of field oscillation may encompass eight unit cells. Also, on the rectangular lattice, the field components usually consist of dipoles that are elongated in the *x* direction. As the modal order increases, these dipoles tend to adopt more complex structure. On the other hand, the square lattice's field adopts complexity through both dipole and quadrupole behavior centered in the each cell, vein spot or vein midpoint. There is also a phase difference observed for the rectangular lattice, but in the *x* direction, the difference is comprised of several cell widths. The reason for the field behavior observed for the rectangular lattice is likely due to field concentration caused by the close spacing of the dielectric veins in the *y* direction. Recall that a unit cell is about 26% as wide as it is long. Since the electric field tends to reside mostly within the higher dielectric material, the close spacing tends to elongate the field in the *x* direction making band gap formation difficult, especially for lower values of ε. It is necessary to get the dielectric and air bands to separate in order for band gaps to form. It simply does not happen for the rectangular lattice under these conditions. Still, it is important to say that this assertion is merely conjecture, not proof.

4.6 Example Calculation Set at the Micron Scale

Preceding discussions have presented a modal analysis of electromagnetic wave propagation within dimensionless 2D square and rectangular vein crystal lattices for two different relative dielectric permittivity values. In this section, we apply dimensions to the rectangular model and deduce the wavelengths of light propagated for different wave vectors existing at the border of the Brillouin zone. The selection of a particular k-point implies a propagation direction for the mode. Since mirror symmetry is enforced in this study, all modes

(electromagnetic waves) are confined to the *xy*-plane. The wavenumber *k* for the mode is simply derived as the magnitude of the wave vector, i.e.,

$$k = |\,\mathrm{k}\,| = \sqrt{k_x^2 + k_y^2 + k_z^2} \tag{49}$$

From the wavenumber, we can easily determine the wavelength λ for the mode. To do so, we use the formula

$$\lambda = \frac{2\pi}{k} \tag{50}$$

For dimensionless input, the MPB computer code produces dimensionless output.[2] This procedure offers great utility since dimensionless solutions can be scaled into any system of units desired. The dimensionless wave vector $\bar{\mathrm{k}}$ may be expressed in terms of the dimensioned wave vector k as follows

$$\bar{\mathrm{k}} = \frac{\mathrm{k}\,a}{2\pi} \tag{51}$$

The dimensionless angular frequency $\bar{\omega}$ is expressed in terms of the dimensioned angular frequency by the formula

$$\bar{\omega} = \frac{\omega a}{2\pi c} \tag{52}$$

where *c* is the speed of light in vacuum, approximately 2.997×10^8 m/s. Equations (51) and (52) may be used to convert $\bar{\mathrm{k}}$ and $\bar{\omega}$ into their dimensioned equivalents.

For a specific example regarding the lattice shown in Figure 6, the lattice constant is set to 0.333 μm (or 0.333×10^{-6} m). By sweeping over the wave vectors at the edge of the Brillouin zone shown in Figure 7, we obtain the range of wave numbers and wavelengths shown in Figure 30 for $\varepsilon = 8.90$. As is evidenced by Figure 30, for the selection of wave vectors, the rectangular lattice mostly admits light waves in the range of 0.25 μm to 3.5 μm with corresponding wave numbers between 0 rad/μm to 40 rad/μm. The wavelength range is of course broader than that stated due to the singularity at *k* = 0. Recall that the Brillouin zone does include the wave vector $\mathrm{k} = (0,0,0)$. The frequency loci can also be transformed into a common system of units for each mode. Figure 31 contains this plot for $\varepsilon = 8.90$.

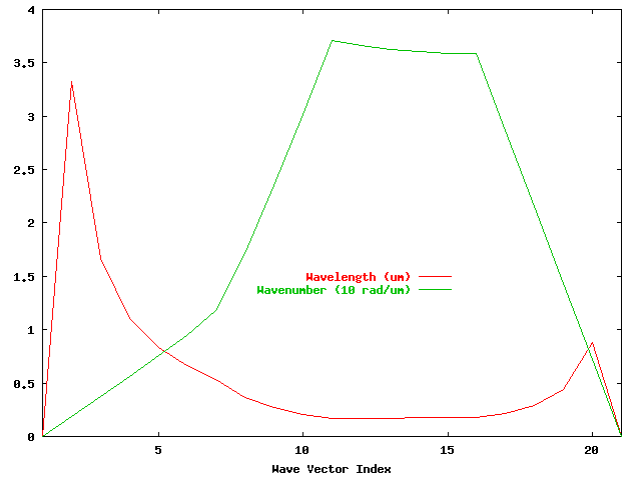

Figure 30. Wavelengths and wave numbers predicted for a rectangular lattice with lattice constant set at 0.333 μm and a vertical aspect ratio of 0.26315. The wavelength unit is micrometers; the wave number unit is tens of radians per micrometer. Relative dielectric permittivity is set at 8.90

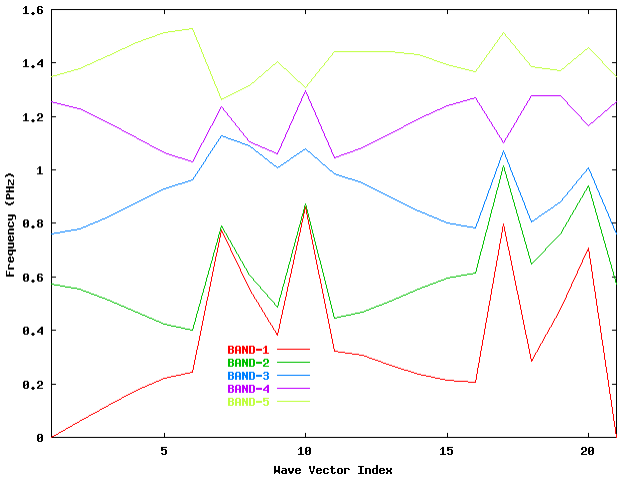

Figure 31. Band or mode frequencies predicted for a rectangular lattice with lattice constant set at 0.333 μm and a vertical aspect ratio of 0.26315, relative dielectric permittivity 8.90. The frequency unit is Petahertz.

The dimensioned frequency plot has an appearance that is identical to that for the dimensionless frequency graph shown in Figure 8. Now real frequency units are assigned. Similar calculations can be performed on the same lattice with $\varepsilon = 1.52$. The resulting wavelength and wave number distributions are the same as shown in shown in Figure 30 since the Brillouin zone is the same. The attendant frequency plot is provided in Figure 32. On the whole, a major effect of reducing the relative permittivity on the rectangular lattice is to elevate the modes to higher frequencies and to increase the jaggedness of the frequency plots. In some cases, the separation in frequency between modes also shrinks. In terms of light coloration, this example largely involves light in the wavelength range of 0.25 μm to 3.5 μm (250 nm to 3,500 nm). For the first Brillouin zone, this band is roughly concurrent with the visible spectrum and the near infrared. As one may conclude, this solution procedure renders a wealth of information on the behavior of electromagnetic radiation in the photonic crystal and allows very precise control over wave number and frequency combinations for research consideration.

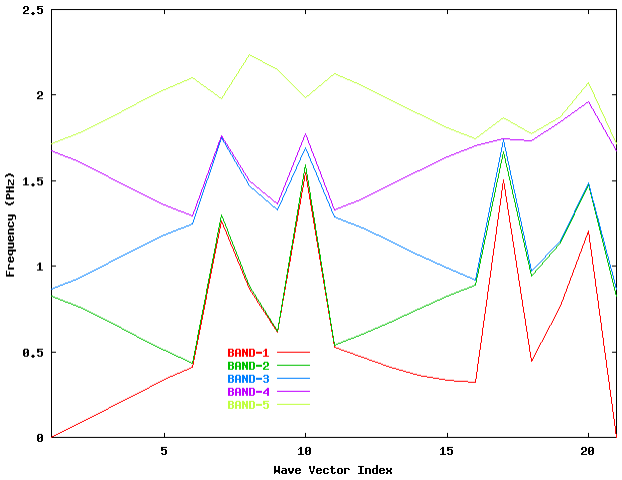

Figure 32. Band or mode frequencies predicted for a rectangular lattice with lattice constant set at 0.333 μm and a vertical aspect ratio of 0.26315, relative dielectric permittivity 1.52. The frequency unit is Petahertz.

5 CONCLUSIONS

A frequency-based solution method for the propagation of electromagnetic waves has been discussed in this report. Specifically, modal frequencies and shapes for square and rectangular 2D photonic crystals have been calculated for two different relative dielectric permittivity values. In this study, the high permittivity values are confined to dielectric veins. A principal result is that for the high permittivity case, a band gap exists for the square lattice in both the transverse electric and magnetic waves. No such gaps exist for the specific rectangular lattice (rectangular ratio - 1:0.26) considered here. For the low permittivity analyses, no band gaps exist for either lattice. These calculations may be repeated for the higher permittivity value $\varepsilon = 2.31$ in direct correspondence with a proper value for chitin. However, this oversight has little impact on the results. The frequencies are affected only to a small degree for the higher order modes. Details concerning the electric field components have been discussed for each lattice. Significant differences between electric fields for the square and rectangular lattices have been highlighted. The level of field compression caused by the close spacing of dielectric veins seems to cause waves on the rectangular lattice to depart from those observed for the square lattice. A point of future interest may be to determine what minimal changes need be made to the rectangular lattice in order to motivate the appearance of band gaps. We may also continue to add geometric complexity to the rectangular lattice in order to make it better representative of the butterfly wing lattice introduced early in this report. Such investigations are under consideration for a forthcoming program of research. As a collateral benefit, this project has served to exercise the author's skills both in utilizing MPB in working with the equations of electromagnetism. Musculature for the latter has sadly atrophied a bit with the passage of time.

REFERENCES

1. Kawano, K. and Kitoh, T., *Introduction to Optical Waveguide Analysis: Solving Maxwell's Equations and the Schrödinger Equation,* John Wiley & Sons, New York, N.Y., 2001.

2. Joannopoulos, J.D., Johnson, S.G., Winn, J.N. and Meade, R.D., *Photonic Crystals: Molding the Flow of Light*, 2nd Ed., Princeton University Press, Princeton, NJ, 2008.

3. Michielsen, K., De Raedt, H. and Stavenga, D., "Reflectivity of the gyroid biophotonic crystals in the ventral wing scales of the green hairstreak butterfly, *Callophrys rubi*", *J. R. Soc. Interface,* doi: 10.1098/rsif.2009.0352.

4. Leertouwer, H.L., Wilts, B.D. and Stavenga, D.G., "Refractive index and dispersion of butterfly chitin and bird keratin measured by polarizing interference microscopy", *Optics Express*, Vol. 19, No. 24, pp. 24061-24066, 2011.

5. Kittel, C., *Introduction to Solid State Physics*, 8th Ed., John Wiley & Sons, New York, NY, 2005.

6. Fox, M., *Quantum Optics: An Introduction,* Oxford Master Series in Atomic, Optical and Laser Physics, Oxford University Press, Oxford, 2006.

7. Griffiths, D.J., *Introduction to Electrodynamics,* Prentice-Hall, New Jersey, 1981.

8. Jackson, J.D., *Classical Electrodynamics, 3rd Ed.,* John Wiley & Sons, New York, N.Y., 1998.

9. Cunningham, S.L., "Special points in the two-dimensional Brillouin zone", *Physical Review B,* Vol. 10, No. 12, pp. 4988-4994, 1974.

10. Nayak, C., "Solid State Physics", Class Notes on Condensed Matter Physics, University of California – Los Angeles, September 2000.

11. Johnson, S.G. and Joannopoulos, J.D., "Block-iterative frequency-domain methods for Maxwell's equations in a planewave basis", *Optics Express,* Vol. 8, No. 3, 2001.

12. Stoddart, P.R., Cadusch, P.J., Boyce, T.M., Erasmus, R.M. and Comins, J.D., "Optical properties of chitin: surface-enhanced Raman scattering substrates based on antireflection structures on cicada wings", *Nanotechnology,* Vol. 17, pp. 680-686, 2006.

DISTRIBUTION LIST
AFRL-RW-EG-TR-2012-114

Defense Technical Information Center Attn: Acquisition (OCA) 8725 John J. Kingman Road, Ste 0944 Ft Belvoir, VA 22060-6218	1 Electronic Copy (1 file, 1 format)

EGLIN AFB OFFICES:

AFRL/RWOC (STINFO Tech Library Copy)	1 Copy
AFRL/RW CA-N	Notice of publication only
AFRL/RWWI	3 Copies